

## A CONSTITUTIVE MODEL FOR SIMULATING SOIL-CONCRETE INTERFACES

Zhen Chen  
Howard L. Schreyer

New Mexico Engineering Research Institute  
University of New Mexico  
Albuquerque, New Mexico 87196

July 1986

Final Report

DTIC  
ELECTE  
SEP 17 1986  
S R D

Approved for public release; distribution unlimited.

AIR FORCE WEAPONS LABORATORY  
Air Force Systems Command  
Kirtland Air Force Base, NM 87117-6008

86 9 16 051

AD-A171 923



DTIC FILE COPY

This final report was prepared by the New Mexico Engineering Research Institute, Albuquerque, New Mexico, under Contract F29601-84-C-0080, Job Order 2302Y201 with the Air Force Weapons Laboratory, Kirtland Air Force Base, New Mexico. Dr. Timothy J. Ross (NTES) was the Laboratory Project Officer-in-Charge.

When Government drawings, specifications, or other data are used for any purpose other than in connection with a definitely Government-related procurement, the United States Government incurs no responsibility or any obligation whatsoever. The fact that the Government may have formulated or in any way supplied the said drawings, specifications, or other data, is not to be regarded by implication, or otherwise in any manner construed, as licensing the holder, or any other person or corporation; or as conveying any rights or permission to manufacture, use, or sell any patented invention that may in any way be related thereto.

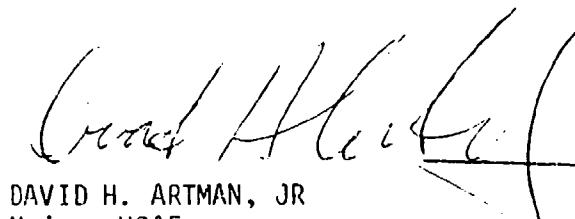
This report has been authored by a contractor of the United States Government. Accordingly, the United States Government retains a nonexclusive, royalty-free license to publish or reproduce the material contained herein, or allow others to do so, for the United States Government purposes.

This report has been reviewed by the Public Affairs Office and is releasable to the National Technical Information Service (NTIS). At NTIS, it will be available to the general public, including foreign nations.

If your address has changed, if you wish to be removed from our mailing list, or if your organization no longer employs the addressee, please notify AFWL/NTES, Kirtland AFB, NM 87117 to help us maintain a current mailing list.

This technical report has been reviewed and is approved for publication.

  
TIMOTHY J. ROSS  
Project Officer

  
DAVID H. ARTMAN, JR  
Major, USAF  
Chief, Applications Branch

FOR THE COMMANDER

  
CARL L. DAVIDSON  
Colonel, USAF  
Chief, Civil Engineering Rsch Division

DO NOT RETURN COPIES OF THIS REPORT UNLESS CONTRACTUAL OBLIGATIONS OR NOTICE ON A SPECIFIC DOCUMENT REQUIRES THAT IT BE RETURNED.

UNCLASSIFIED

SECURITY CLASSIFICATION OF THIS PAGE

## REPORT DOCUMENTATION PAGE

H171923

1a. REPORT SECURITY CLASSIFICATION Unclassified			1b. RESTRICTIVE MARKINGS		
2a. SECURITY CLASSIFICATION AUTHORITY			3. DISTRIBUTION/AVAILABILITY OF REPORT Approved for public release; distribution unlimited.		
2b. DECLASSIFICATION/DOWNGRADING SCHEDULE					
4. PERFORMING ORGANIZATION REPORT NUMBER(S) NMERI WA8-9~(8.09)			5. MONITORING ORGANIZATION REPORT NUMBER(S) AFWL-TR-86-06		
6a. NAME OF PERFORMING ORGANIZATION New Mexico Engineering Research Institute		6b. OFFICE SYMBOL (If applicable) NMERI	7a. NAME OF MONITORING ORGANIZATION Air Force Weapons Laboratory		
6c. ADDRESS (City, State and ZIP Code) University of New Mexico Albuquerque, NM 87131			7b. ADDRESS (City, State and ZIP Code) Kirtland Air Force Base, NM 87117		
8a. NAME OF FUNDING/SPONSORING ORGANIZATION		8b. OFFICE SYMBOL (If applicable)	9. PROCUREMENT INSTRUMENT IDENTIFICATION NUMBER F29601-84-C-0080		
8c. ADDRESS (City, State and ZIP Code)			10. SOURCE OF FUNDING NOS.		
			PROGRAM ELEMENT NO. 62201F	PROJECT NO. 2302	TASK NO. Y2
					WORK UNIT NO. 01
11. TITLE (Include Security Classification) A CONSTITUTIVE MODEL FOR SIMULATING SOIL-CONCRETE INTERFACES					
12. PERSONAL AUTHOR(S) Chen, Zhen; Schreyer, Howard L.					
13a. TYPE OF REPORT Final Report		13b. TIME COVERED FROM Nov 84 TO Nov 85		14. DATE OF REPORT (Yr., Mo., Day) 1986 July	
15. PAGE COUNT 70					
16. SUPPLEMENTARY NOTATION					
17. COSATI CODES			18. SUBJECT TERMS (Continue on reverse if necessary and identify by block number)		
FIELD	GROUP	SUB. GR.			
08	13		Viscoplasticity, Concrete, Soils, Strain Rate, Strain		
11	02		Softening, Interface, Localization, Strain Gradient		
19. ABSTRACT (Continue on reverse if necessary and identify by block number)					
<p>This investigation explores the characteristics of deformation at the interface of dissimilar materials such as concrete and soil. Based upon the basic features of the deformation field, a new nonlocal approach for simulating soil-concrete interfaces is proposed. It is assumed that the stress field is a function of both strain and strain gradients, and also, no relative slip occurs at the contact surface between soil and concrete. By using computational plasticity and the finite element method, static and dynamic responses of the softer material next to an interface are evaluated numerically. Comparisons are made with other numerical data. Conclusions are given on the apparent suitability of the approach.</p>					
20. DISTRIBUTION/AVAILABILITY OF ABSTRACT UNCLASSIFIED/UNLIMITED <input type="checkbox"/> SAME AS RPT <input checked="" type="checkbox"/> OTIC USERS <input type="checkbox"/>			21. ABSTRACT SECURITY CLASSIFICATION Unclassified		
22a. NAME OF RESPONSIBLE INDIVIDUAL Dr. T. J. Ross		22b. TELEPHONE NUMBER (Include Area Code) (505) 844-9087		22c. OFFICE SYMBOL NTESA	

# CONTENTS

<u>Section</u>		<u>Page</u>
I	INTRODUCTION	1
II	SCOPE OF THE INVESTIGATION	3
	Objective	3
	Interface Phenomena	3
	Present Status of Models for Interfaces	6
	Procedure	9
III	MATHEMATICAL MODEL	10
	Assumptions	10
	Basic Equations	11
	A Constitutive Relation for the Interface Under Shear	18
	Features of the Model	18
IV	COMPARISONS WITH OTHER NUMERICAL DATA	25
	Dynamic Response of the Interface Under Shear	25
	Static Response of the Interface Under Shear	45
V	CONCLUSIONS	57
	REFERENCES	58
	LIST OF SYMBOLS	60



Accession For	
NTIS CRA&I	<input checked="" type="checkbox"/>
DTIC TAB	<input type="checkbox"/>
Unannounced	<input type="checkbox"/>
Justification	
By	
Distribution /	
Availability Codes	
Dist	Avail and/or Special
A-1	

## ILLUSTRATIONS

<u>Figure</u>		<u>Page</u>
1	Geometry for the interface problem	4
2	Effect of the parameter $\eta$ in the hardening regime	19
3	Effect of the parameter $a_5$ in the softening regime	20
4	Effect of mean pressure on the stress-strain curve	21
5	Effect of the parameter $a_3$ , or the invariant of strain gradient, on stress-strain response	22
6	Illustrations of loading, unloading, and reloading in the hardening and softening regimes	24
7	Finite element mesh of the soil bar and the shape function used	27
8	Illustration of elastic stress wave at various times	33
9	Spatial distribution of stress at various times	34
10	Spatial distribution of stress at various times using the current approach	35
11	Spatial distributions of displacement field at various times	36
12	Spatial distribution of displacement field at various times using the current approach	37
13	Spatial distribution of strain at various times	38
14	Spatial distribution of strain at various times using the current approach	39
15	Shear stress-strain path for element 1 at time $t = 1.7$	40
16	Shear stress-strain path for element 20 at time $t = 1.7$	41
17	Distribution of displacement at $t = 1.7$ for different meshes	42
18	Distribution of stress at $t = 1.7$ for different meshes	43
19	Distribution of strain at $t = 1.7$ for different meshes	44
20	Strain distribution for static response in elastic regime	47
21	Strain distribution for static response in softening regime	48
22	Stress distribution for static response in softening regime	49
23	Shear stress-strain response of element 1	50

## ILLUSTRATIONS (Concluded)

<u>Figure</u>		<u>Page</u>
24	Shear stress-strain response of element 6	51
25	Shear stress-strain response of element 10	52
26	Strain distribution for different meshes to show convergence	53
27	Effect of the parameter $a_3$ , or the invariant of strain gradient, on the static response near the surface	54
28	Shear stress versus the displacement of the end of the soil bar for various values of mean pressure	56

## I. INTRODUCTION

Because of failures in structures caused by ground motion from earthquakes or explosives, soil-concrete interaction problems are playing an increasingly important part in engineering design procedures and safety analyses. The information available, however, is still sparse due to the complexity of the nonlinear response of these geologic materials.

In the past, many models for representing interfaces were based on Coulomb's law, i.e., no slip between two bodies will occur unless a critical tangential stress is reached, and the relative motion is constrained to be along the contact surface if the critical state is reached. For dissimilar materials like concrete and soil, however, Coulomb's law may not be applicable, since slip does not occur at the interface. Instead of slip, a band with large shear deformation is observed in the weaker of the two materials, and these observed zones with large strain gradients cannot be automatically predicted. Nevertheless, the simple friction approach has been utilized with either slip lines or special interface elements to obtain computational procedures, which in turn introduce questions of stability and computational complexity.

This research addresses a new approach for simulating a soil-concrete interface where both theoretical and computational aspects are kept in mind. The idea relies on the observations that (1) slip does not occur for the soil-concrete interface until a failure state is reached, and that (2) progressive, distributed damage produces a band of permanent deformation in the soil adjacent to the interface. The lateral dimension of the band appears to depend on the physical characteristics of the materials. The only way to predict a finite zone of localized deformation under a homogeneous state of stress is to utilize a nonlocal constitutive law. Furthermore, it appears that localization occurs only when softening is present. Thus, if a nonlocal constitutive model is postulated where softening is governed by both strain and the gradient of strain, then softening localizes into a finite region, which cannot be predicted by using a local constitutive model. With the use of a nonlocal constitutive model for soil, and the assumption that the interface initiates softening in the weaker of the two materials, the deformation field adjacent to the interface can be simulated.

In this study, numerical solutions of a model problem with dynamic and static shear loadings are compared with other numerical data. It was conclude that the new approach is reasonable in an engineering sense, and it is feasible to incorporate the model into existing finite element and finite difference computer codes.



## II. SCOPE OF THE INVESTIGATION

### OBJECTIVE

Based on existing experimental data, the general behavior of soil adjacent to a concrete interface can be described. Some assumptions are proposed to construct a new nonlocal constitutive model for simulating the behavior of soil in the vicinity of an interface. Using computational plasticity theory, the characteristics of the model are discussed. Existing theoretical data are used for comparison with the model. Conclusions and comments on possible future research are given.

### INTERFACE PHENOMENA

Interface behavior has drawn considerable attention in recent years, especially for the following engineering problems: retaining wall design, skin friction in piles, soil-structure interaction for nuclear power plants subjected to earthquake loadings, and for underground structures subjected to blast and ground shock.

Due to the limitations of experimental techniques, and the assumptions that Coulomb's friction principle holds for interfaces of deformable bodies, there have been a limited number of investigations of interface phenomena. Existing experimental data do not provide an accurate view of the deformation field in the vicinity of the interface. Nevertheless, an approximate description and some knowledge of the soil-concrete interface can be obtained by carefully analyzing the data. This research discusses the problem from a continuum point of view and presents an alternate viewpoint based on the observation that, adjacent to an interface, a region with a large gradient of strain is often formed for shear loading (Fig. 1). An important part of this work was to develop a procedure for describing this phenomenon.

Among the investigators dealing with soil-concrete interface phenomena, Huck, et al., (Refs. 1 and 2), were unique in that both experimental and analytical investigations were performed. Also, several valuable references were given. From their interface tests under static and dynamic shear loadings, it was concluded that interface shear resistance is strongly influenced by the

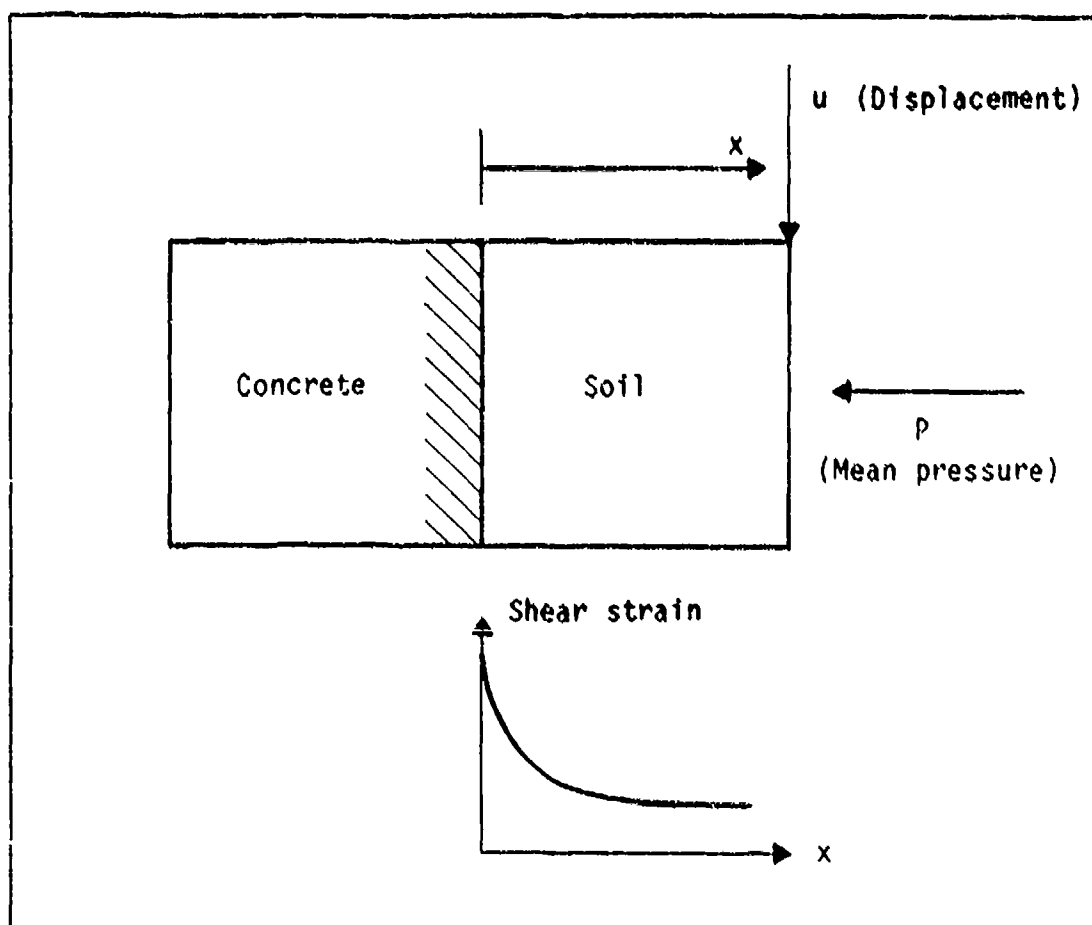


Figure 1. Geometry for the interface problem.

soil type, the stress normal to the interface, and the relative size of the interface roughness with respect to the soil grain diameter. Total interface shear resistance is reduced below the soil shear strength due to softening of the expansive soil and loss of adhesion. It appears that localization of large deformations usually occurs adjacent to the interface, in a region characterized as a shear band, which increases gradually in thickness with continued increase in applied static displacement. After each interface test, the final dimension of the band of permanent deformation is not the same for different materials.

Drumm and Desai (Ref. 3) worked on soil-structure interface tests under static and cyclic loadings by using a new testing apparatus called the "Cyclic Multi-Degree-of-Freedom" device. They indicated that the behavior of a structure resting on, or embedded in a foundation depends on the material properties of both the structure and the foundation medium, and on the types of applied loadings. Soil-structure interaction becomes more significant when structures are subjected to dynamic loadings. The interface strength was found to be less than that of soil, and gradual separation may occur at or near the interface.

Vermeer (Ref. 4) investigated interface behavior between granular materials and metals during powder compaction in a die. There are two friction angles in powder compaction: one for powder-wall friction, and another for powder-powder friction. These two angles were shown to be related for compaction in a die with rough walls. From tests, it was pointed out that the powder-wall slip plane is in fact a thin shear band.

A number of factors, not directly pertinent to the basic soil-concrete interface problem, might act to obscure the true phenomena. However, by analyzing the experimental apparatus and test results mentioned above, it was possible to draw the following descriptions for the mechanism of an interface consisting of concrete and particulate material.

Imperfections at or near the soil-concrete interface will initiate progressive distributed damage such as dispersed microcracking, void formation, or loss of interparticle contacts. From the macroscopic viewpoint, large deformations can be observed adjacent to the interface, and the size of

the band of permanent deformation will enlarge with increase in the applied displacement. Although relative motion occurs between particles as soon as external loading is applied, no slip seems to occur as the stress is increased. If deformation continues to increase, the stress will reach a peak and then decrease in what is called the postpeak regime. Slip appears to be initiated somewhere in the postpeak regime. When macroscopic slip occurs, the dimension of the band seems fixed and the total deformation field is not continuous. Thus, slip might be considered as a mechanism that occurs after the formation of the shear band.

#### PRESENT STATUS OF MODELS FOR INTERFACES

During the past 20 years, evaluation of the dynamic interaction between a structure and the surrounding medium has been accomplished by two approaches, consisting of either the use of classical continuum mechanics, or the finite element method.

The first approach simulates the effects of soil on the structural response by a series of springs and dashpots representing a theoretical half space surrounding the structure. This method is generally limited to elastic or viscoelastic representations of soils. The finite element method is an alternative approach to solving problems in continuum mechanics. Although based on the same principles of mechanics, it changes the partial differential equations governing the motion of the continuum into a finite set of ordinary differential equations in the time domain which makes it possible to incorporate a more reasonable constitutive relation into the interface model. A survey of both the spring-dashpot and finite element approaches to the structure-soil interaction problem was given by Hadjian, et al., (Ref. 5). Also, Seed, et al., (Ref. 6), presented an evaluation of the strengths and weaknesses of the two approaches. Although the above information reviewed only the efforts in an infant period of research, the history of development in this field was quite helpful.

Recently, emphasis in research has been on improving the description of interface behavior, not only in the prepeak regime, but also in the postpeak regime, while computer-based techniques have supplied powerful tools for analyses. Mathematical models are set up with the use of both conservation

principles and constitutive relations. Conservation principles, based upon classical physics, or Newtonian physics, have been well established. Hence, accurate descriptions of the behavior of materials have become more and more important. Desai and Siriwardane (Ref. 7) reviewed and explored the constitutive behaviors of engineering materials, with emphasis on geological materials such as soil and concrete. Currently, in addition to the classical continuum approach for soil-concrete interface, both the particle approach, together with statistical analysis, and the nonlocal continuum approach have been proposed.

Huck, et al., (Refs. 1 and 2), derived a soil-concrete interface model using basic frictional mechanisms as applied to a particulate soil. The particle approach employed the mechanisms of adhesion, plowing, and lifting. The concrete interface surface was considered as a flat plane, with protruding spherical caps representing the roughness or asperities of the concrete surface. Soil in contact with the concrete interface was modeled as spherical particles of known size, but randomly distributed over the interface surface. In the model, relative slip between soil and concrete occurred if, and only if, a critical tangential stress was reached, and the relative motion was assumed to be along the contact surface. The tangential stress was proportional to the normal stress. It appears that gradual formation of a shear band could not be predicted. This constitutive model is, by nature, a classical Mohr-Coulomb model.

Vermeer (Ref. 4) investigated interface response in powder compaction by means of a nonassociated perfect-plasticity model. The idea of sliding on a single plane was considered much too restrictive. Therefore, a new idea allowed small slipping motions on an infinite number of closely spaced parallel surfaces, and used the Mohr-Coulomb criterion. To calculate the stress and density distributions at several stages of the loading process, three approaches were suggested. The first was the use of a nonassociated constitutive model and a fine mesh near the walls of the die, so that a thin shear band could develop. The second consisted of special thin interface elements to model the shear band along the wall. Frictional sliding was implemented directly as a mixed boundary condition in the third approach.

Drumm and Desai (Ref. 3), and Oden and Pires (Ref. 8), describe the constitutive behavior of the interface by using frictional principles with some modifications. Either elasticity or perfectly-plastic relations have been used for simulating soil-concrete interface by these authors as well as others.

From the research efforts mentioned above, it was found that assumptions based upon frictional theories were commonly adopted, and numerical methods are under active development to solve the continuum models. It is doubtful, however, that frictional theories are useful for representing interfaces involving materials with disparate properties such as concrete and soil. In addition, there are some unpleasant features associated with numerical procedures for frictional models, such as size-dependent response and computational difficulties due to special algorithms. To obtain a basic understanding of the inherent physical nature of the interface, and to apply the knowledge to engineering practice, the exploration of a more reasonable and convenient approach seems necessary.

With the development of knowledge for heterogeneous materials, a nonlocal continuum theory offers hope for modeling the postpeak behavior of geological materials. The word "nonlocal" in this context means that stress depends both on strain and strain distribution. The latter can be given through the use of integrals and a weighting function, or by derivatives of strain. The full force-deformation behavior, but not necessarily the stress-strain relationship, beyond peak stress has been documented for concrete, rock, soils, and some other materials under uniaxial stress. One approach was to model the postpeak behavior by using plasticity and the reduction of stress with strain. However, serious theoretical and computational difficulties caused by strain softening have occurred, and they have been intensely debated at recent conferences. Valanis (Ref. 9), Sandler and Wright (Ref. 10), and Read and Hegemier (Ref. 11) discussed in detail the various arguments concerning strain softening. Bazant, et al., (Ref. 12), incorporated strain softening into a constitutive model by using a nonlocal continuum theory. Schreyer and Chen (Ref. 13) investigated the effects of strain softening and localization in a structure by assuming that stress was a function of both strain and strain gradients. It was concluded that current experimental techniques could not rule out strain softening because instrumentation has not been designed to identify localization and to measure strains in the resulting small zones.

Also, several types of nonlocal approaches have overcome obstacles caused by strain softening. At present, (1) a finite strain-softening zone, (2) nonzero energy dissipation, and (3) numerical stability of dynamic problems have been achieved. Additional research is required to generalize the theory on strain softening. Incorporating strain softening into constitutive models would be useful and feasible in engineering practice if the response of a material can be predicted.

Considering the interface phenomena, it has been suggested that a one-dimensional model (Ref. 13) be used to simulate the weaker of two materials at an interface, with the assumption that an interface, in effect, weakens the softer material. If an interface can be dealt with in such a manner, then special algorithms would not be necessary to handle interfaces, and furthermore, a band of permanent deformation adjacent to the interface will be predicted which is representative of physical behavior. Using conventional, constitutive-equation algorithms and finite-element methods, static and dynamic response features of the interface can be obtained with a simple, convenient calculation.

Since an ultimate objective is to have a completely general model, this research provides a three-dimensional formulation. However, applications are limited to the one-dimensional case.

#### PROCEDURE

Several assumptions are proposed based upon existing experimental data. A three-dimensional constitutive model is then developed for simulating the soil-concrete interface by the use of nonlinear plasticity theory. The model reflects the characteristics of geological materials more accurately than a bilinear constitutive model. Features of the model are explored under different values of mean pressure and strain gradient. In order to verify the model for an interface under dynamic shear loading, the finite element method is used, together with explicit time integration and computational plasticity techniques, to obtain numerical solutions which are compared with existing theoretical data for the wave propagation problem. The conclusion of this research shows results for static shear loading.

### III. MATHEMATICAL MODEL

#### ASSUMPTIONS

Making assumptions was the first nontrivial step in the formulation of the new model. Reasonable assumptions yield good results with a modest effort, whereas poor assumptions can lead to considerable computational effort. Making good assumptions depends on engineering experience and intuition. Furthermore, each assumption has its own limitation which must correspond to the problems being considered.

As mentioned previously, there is not enough experimental data to provide a good qualitative description of the behavior at soil-concrete interfaces. For example, it is still uncertain at what stage of the loading path the macroscopic slip between concrete and soil occurs, if it occurs at all. The following assumptions were made to construct a new nonlocal continuum model, which is different from the usual Mohr-Coulomb model.

Assumption 1--Slip does not occur at the contact surface between concrete and soil under shear loading. Instead, with an increase in load, a shear band will form due to dispersed microcracking. This shear band represents a localization of deformation that is accompanied by softening.

Assumption 2--The imperfection of the soil-concrete interface reduces the strength of the soil, so that with large enough loads, the softening is initiated in the region of soil adjacent to the interface. With this assumption, the roughness of the concrete surface is simulated through the strength property of the adjacent material, rather than through a friction coefficient. The result is that softening is initiated at a lower load for a smooth interface compared to a rough interface, but the evolution of softening and the localization zone will be governed by the constitutive equation.

Assumption 3--A nonlocal constitutive theory is required to represent the localized behavior of softening in soil. This theory provides a means for controlling the size of the localization.

Assumption 4--A suitable nonlocal theory is obtained if the limit stress depends on the strain gradient. Read and Hegemier (Ref. 11) indicated that



strain softening is not a true material property, but is simply a manifestation of the effects of progressively increasing inhomogeneity of deformation. However, an alternate interpretation, that equally explains the observed phenomena, is that softening occurs only in the presence of strain gradients. The assumption that limit stress reduces with the strain gradient is therefore a simple mathematical representation of the observation.

## BASIC EQUATIONS

To simulate the general constitutive behavior of soil-concrete interfaces, a nonassociated Prager-Drucker model, with some modifications, was adopted to provide appropriate inelastic response features of soils. Such a model does not accurately reflect the behavior of soils, but it is one of the simplest inelastic models that can be used. If strain gradients are incorporated into a complex model, it becomes difficult to separate and study the various features individually.

In the theory of plasticity (Ref. 14), the case of combined stresses is represented by means of the concept of a yield surface. For any point in a material region, assume that there exists a domain in the stress space in which material behavior is governed by elasticity theory. The hypersurface bounding this domain is known as the yield surface. If the material is perfectly plastic, the yield surface does not move. If the yield surface expands out to a limit state, the material is said to harden, while the material starts to soften as soon as the yield surface contracts in a controlled manner. The motion of the surface is governed by internal variables which record that part of the stress history involving inelastic behavior and other variables directly affecting yield. The motion of the stress point inside the surface, i.e., in the elastic domain, is not dependent on internal variables. In the general constitutive model used in this research, the internal variables considered included an inelastic strain invariant  $\bar{\epsilon}^i$ , the mean pressure  $P$ , and a strain gradient invariant  $\bar{g}^i$ . The indicial notation was preferred, because this notation allowed us to write equations in a much shorter form than would otherwise be possible. In representations of first and second order tensors, subscripts refer to the indicial notation, while superscripts imply the definitions of tensors, e.g., the elastic or inelastic part of the strain tensor.

In the following part of this subsection, the modified Prager-Drucker yield-surface function is discussed first; then the potential function and some important formulae are given. To solve the nonlinear constitutive equation, an incremental numerical procedure is described based upon computational plasticity theory.

For convenience in numerical calculations, the yield surface is defined in a dimensionless form as:

$$F = \frac{\bar{\sigma} - (1 + a_1 P) G_r H}{\sigma_{LS}} = 0 \quad (1)$$

in which  $\sigma_{LS}$  is the limit value of the shear stress-shear strain curve, and  $\bar{\sigma}$  is the second invariant of deviatoric stress  $\sigma_{ij}^d$  as follows:

$$\bar{\sigma} = \left( \frac{3}{2} \sigma_{ij}^d \sigma_{ji}^d \right)^{1/2} \quad (2)$$

$$\sigma_{ij}^d = \sigma_{ij} - \frac{1}{3} \sigma_{kk} \delta_{ij} \quad (3)$$

The function  $H$  incorporates both strain hardening and softening according to the following relations:

$$H = L_0 + (L_p - L_0) \sin \left[ \frac{\pi}{2} \left( \frac{\bar{e}^i}{\bar{e}_L^i} \right)^n \right] \quad 0 \leq \bar{e}^i \leq \bar{e}_L^i \quad (4)$$

$$H = (L_p - a_4) \left( 1 + a_5 \frac{\bar{e}^i - \bar{e}_L^i}{\bar{e}_L^i} \right) e^{-a_5 \frac{\bar{e}^i - \bar{e}_L^i}{\bar{e}_L^i}} + a_4 \quad \bar{e}^i > \bar{e}_L^i \quad (5)$$

The total strain tensor is divided into an elastic part and an inelastic part, as follows:

$$e_{ij} = e_{ij}^e + e_{ij}^i \quad (6)$$

Then, one of the internal variables in Eqs. 4 and 5, the inelastic strain invariant is:

$$\bar{\epsilon}^i = J \left( \frac{2}{3} de_{ij}^{di} de_{ji}^{di} \right)^{1/2} \quad (7)$$

where

$$e_{ij}^{di} = e_{ij}^i - \frac{1}{3} e_{kk}^i \delta_{ij} \quad (8)$$

The values of  $H$  at initial yield and the limit state are denoted by  $L_0$  and  $L_p$ , respectively. The value of  $\bar{\epsilon}^i$  at the limit state,  $\bar{\epsilon}_L^i$ , is assumed to be independent of path. The parameter  $n$  controls the shape of the stress-strain relation in the hardening regime while  $a_3$  controls the shape during softening. The softening formulation for  $H$  given in Eq. 5 provides a horizontal slope at the limit state and a limiting value for  $H$  of  $a_4$  for large  $\bar{\epsilon}^i$ .

The invariant  $(\bar{g}^i)$  of the strain gradient is defined by the relation:

$$\bar{g}^i = \left( e_{kl,1}^i e_{kn,n}^i \right)^{1/2} \quad (9)$$

The strain-gradient factor,  $G_r$ , in Eq. 1 is assumed to be of the form

$$G_r = (1 - a_2) e^{-a_3 \bar{g}^i} + a_2 \quad (10)$$

where the parameter  $a_3$  controls the rate at which  $G_r$  decreases with  $\bar{g}^i$ . For  $\bar{g}^i$  equal to zero,  $G_r$  is unity, and for large  $\bar{g}^i$ , the function  $G_r$  asymptotically approaches  $a_2$ .

To be consistent with experimental data (Refs. 1, 3, and 7) for geological and other frictional materials, the mean pressure

$$P = - \frac{1}{3} \sigma_{ii} \quad (11)$$

was also incorporated into the constitutive model as a coefficient of the parameter  $a_1$ .

With the use of a nonassociated flow rule, the inelastic part of the strain tensor is given by

$$de_{ij}^i = d\lambda \frac{\partial \phi}{\partial \sigma_{ij}} \quad (12)$$

where the potential function was chosen to be

$$\phi = \frac{\bar{\sigma} - H}{\sigma_{LS}} \quad (13)$$

so that the inelastic strain tensor contains no volumetric component. This is consistent with metal plasticity but is not entirely appropriate for soils which display inelastic volumetric strain. The inclusion of inelastic volumetric strain would have provided a complication that has no direct relationship to softening and localization.

The elastic part of the strain tensor is related to the stress tensor through the elastic constitutive equation:

$$\sigma_{ij} = C_{ijkl} e_{kl}^e \quad (14)$$

where the tensor  $C_{ijkl}$  is normally restricted to the isotropic case.

Now the general constitutive model is established. This model is linear in the elastic regime, and nonlinear in the hardening and softening regimes. Mean pressure increases the strength of the material, while strain gradient reduces its strength.

In the numerical procedure, an incremental scheme was adopted to solve the nonlinear constitutive model. The incremental relations are summarized below:

$$\Delta e_{ij} = \Delta e_{ij}^e + \Delta e_{ij}^i \quad (15)$$

$$\Delta \sigma_{ij} = C_{ijkl} \Delta e_{kl}^e \quad (16)$$

$$\Delta e_{ij}^i = \Delta \lambda \frac{\partial \phi}{\partial \sigma_{ij}} \quad (17)$$

$$\Delta \bar{e}^i = \left( \frac{2}{3} \Delta e_{ij}^{di} \Delta e_{ji}^{di} \right)^{1/2} \quad (18)$$

In practice, the total strain increment  $\Delta e_{ij}$ , the total strain from the previous step  $(e_{ij})_p$ , and the stress from the previous step  $(\sigma_{ij})_p$  are known. The difficult problem is that the elastic and inelastic part of  $\Delta e_{ij}$  are unknown. To solve the above nonlinear equations with unknowns  $e_{ij}$ ,  $\sigma_{ij}$ ,  $e_{ij}^i$ ,  $\Delta \lambda$ , and  $\Delta e_{ij}^i$ , an iterative procedure was used. The basic ideas are those of computational plasticity (Ref. 14). The following is an outline of the constitutive equation algorithm.

Step 1--The user inputs components of the total strain increment tensor, material parameters, and other control parameters. Existing values of stress, total strain, elastic strain and inelastic strain tensors are stored as  $(\sigma_{ij})_p$ ,  $(e_{ij})_p$ ,  $(e_{ij}^e)_p$ , and  $(e_{ij}^i)_p$ , respectively.

Step 2--First, assume that the step is elastic:

$$\Delta e_{ij}^e = \Delta e_{ij}$$

Step 3--For future use, calculate:

$$\bar{\sigma} = \left( \frac{3}{2} \sigma_{ij}^d \sigma_{ji}^d \right)^{1/2}$$

$$T_{ij} = \frac{\partial \phi}{\partial \sigma_{ij}} = \frac{3}{2} \frac{\sigma_{ij}^d}{\sigma_{LS} \bar{\sigma}}$$

$$F' = \frac{\partial F}{\partial \Delta \lambda} = \frac{\partial \phi}{\partial \sigma_{ij}} C_{ijkl} \frac{\partial \phi}{\partial \sigma_{kl}}$$

$$I = 0 \quad (I = \text{iteration count})$$

Step 4--Find increments in stress components:

$$\Delta\sigma_{ij} = C_{ijkl} \Delta e_{kl}^e$$

Step 5--Update old stress components and the iteration count:

$$\sigma_{ij} = (\sigma_{ij})_p + \Delta\sigma_{ij}$$

$$I = I + 1$$

Step 6--Evaluate  $\bar{\sigma}$  and the yield function  $F$ .

Step 7--Check the yield function  $F$ :

(a) If  $F < 0$  and  $I = 1$  (i.e., the first step), then the solution is elastic and the stresses are correct. Go to Step 12.

Otherwise,

(b) If  $|F| < \epsilon$  and  $I > 1$ , then the plasticity solution has been obtained and the stresses are correct. Go to Step 12.

Otherwise, go to Step 8.

Step 8--The iteration begins. The following procedure is used to solve for  $\Delta\lambda$ :

For the first step, ( $I = 1$ ):

$$(\Delta\lambda)_1 = - \frac{(F)_1}{(F')_1} \text{ (one-step Newton-Raphson procedure)}$$

For other steps ( $I > 1$ ):

$$(F')_I = \frac{(F)_I - (F)_{I-1}}{(\Delta\lambda)_{I-1}} \text{ (backward finite difference)}$$

$$(\Delta\lambda)_I = \frac{(F)_I}{(F')_I} = \frac{(\Delta\lambda)_{I-1} (F)_I}{(F)_{I-1} - (F)_I}$$

Step 9--Update inelastic strain increments:

$$(\Delta e_{ij}^i)_I = (\Delta e_{ij}^i)_{I-1} + (\Delta \lambda)_I T_{ij}$$

Step 10--Recalculate elastic strain increments:

$$(\Delta e_{ij}^e)_I = (\Delta e_{ij}^e)_{I-1} - (\Delta \lambda)_I T_{ij}$$

Step 11--Go to Step 4.

Step 12--Update inelastic strain tensor:

$$e_{ij}^i = (e_{ij}^i)_p + \Delta e_{ij}^i$$

Step 13--Compute inelastic strain invariants:

$$\Delta \bar{e}^i = \left( \frac{2}{3} \Delta e_{ij}^{di} \Delta e_{ji}^{di} \right)^{1/2}$$

$$\bar{e}^i = (\bar{e}^i)_p + \Delta \bar{e}^i$$

Step 14--Update elastic strain and total strain tensors:

$$e_{ij}^e = (e_{ij}^e)_p + \Delta e_{ij}^e$$

$$\Delta e_{ij} = \Delta e_{ij}^i + \Delta e_{ij}^e$$

$$e_{ij} = (e_{ij})_p + \Delta e_{ij}$$

Step 15--Exit for next increments of total strain tensor components.

In the algorithm described above, the accuracy and number of iterations are controlled through the magnitudes of the convergence parameter  $\epsilon$  and the increments of total strain. Small values of  $\epsilon$  require generally more iterations and, hence, more computer time. This algorithm is simple and appears to be effective in an engineering sense.

## A CONSTITUTIVE RELATION FOR THE INTERFACE UNDER SHEAR

The constitutive model needs only to be one-dimensional for the soil-concrete interface under shear loading as shown in Fig. 1, and can be derived directly from the above general equations. The stress state of the problem is:

$$\sigma_{11} = \sigma_{22} = \sigma_{33} = \sigma_{23} = \sigma_{13} = 0 \quad (19)$$

The use of Eq. 19 results in the relations:

$$\sigma_{12} = \frac{E}{2(1+\nu)} e_{12}^e \quad (20)$$

$$e_{12} = e_{12}^i + e_{12}^e \quad (21)$$

$$F = \frac{\sqrt{3} \sigma_{12} - H(1+a_1P) \left[ (1-a_2)e^{-a_3\bar{g}^i} + a_2 \right]}{\sigma_{LS}} = 0 \quad (22)$$

$$de_{12}^i = d\lambda \frac{\partial \phi}{\partial \sigma_{12}} \quad (23)$$

To simulate the behavior of soil-concrete interfaces, Eqs. 20-23 are used to represent the constitutive characteristics of soil, and the interface is assumed to initiate failure. The following subsection illustrates the effects of mean pressure and strain gradients on the model through the use of the constitutive equation subroutine. The results should be helpful for understanding the global behavior of a soil-concrete interface.

### FEATURES OF THE MODEL

A total of eight parameters in Eq. 22 can be used to simulate different types of materials. Among these parameters,  $L_0$  and  $L_p$  are the elastic limit and the peak value of the shear stress-strain curve respectively, while  $a_2$  and  $a_4$  are chosen so stress will not be null in the postpeak regime, a reasonable assumption based on experimental observations. Parameters  $a_1$ ,  $a_3$ ,  $a_5$ , and  $n$ , control the basic shape of the stress-strain curve. For the purpose of illustration, the effects of these four parameters are shown separately in Figures 2, 3, 4, and 5 in which stress has been normalized with respect to the



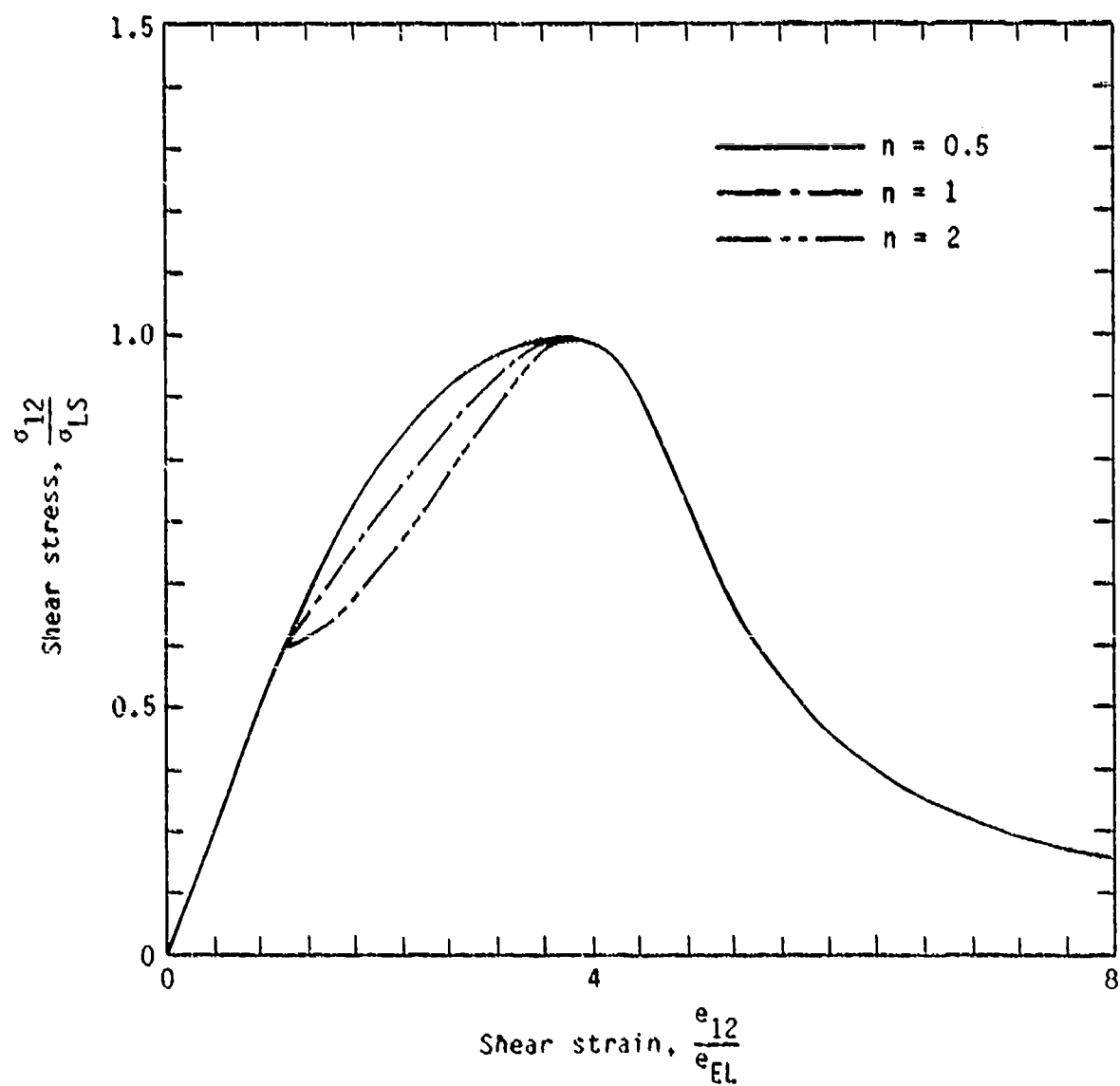


Figure 2. Effect of the parameter  $n$  in the hardening regime.

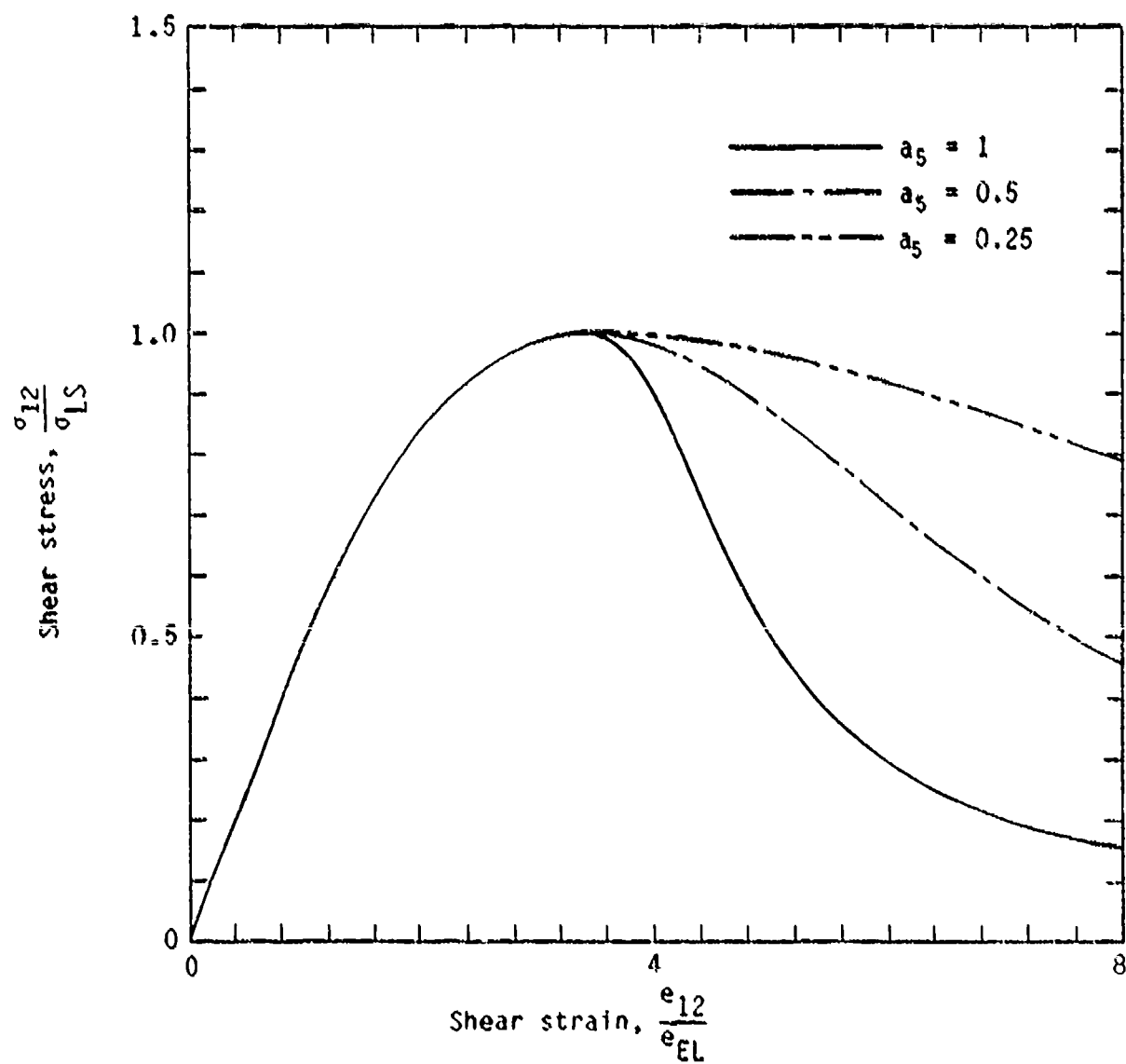


Figure 3. Effect of the parameter  $a_5$  in the softening regime.

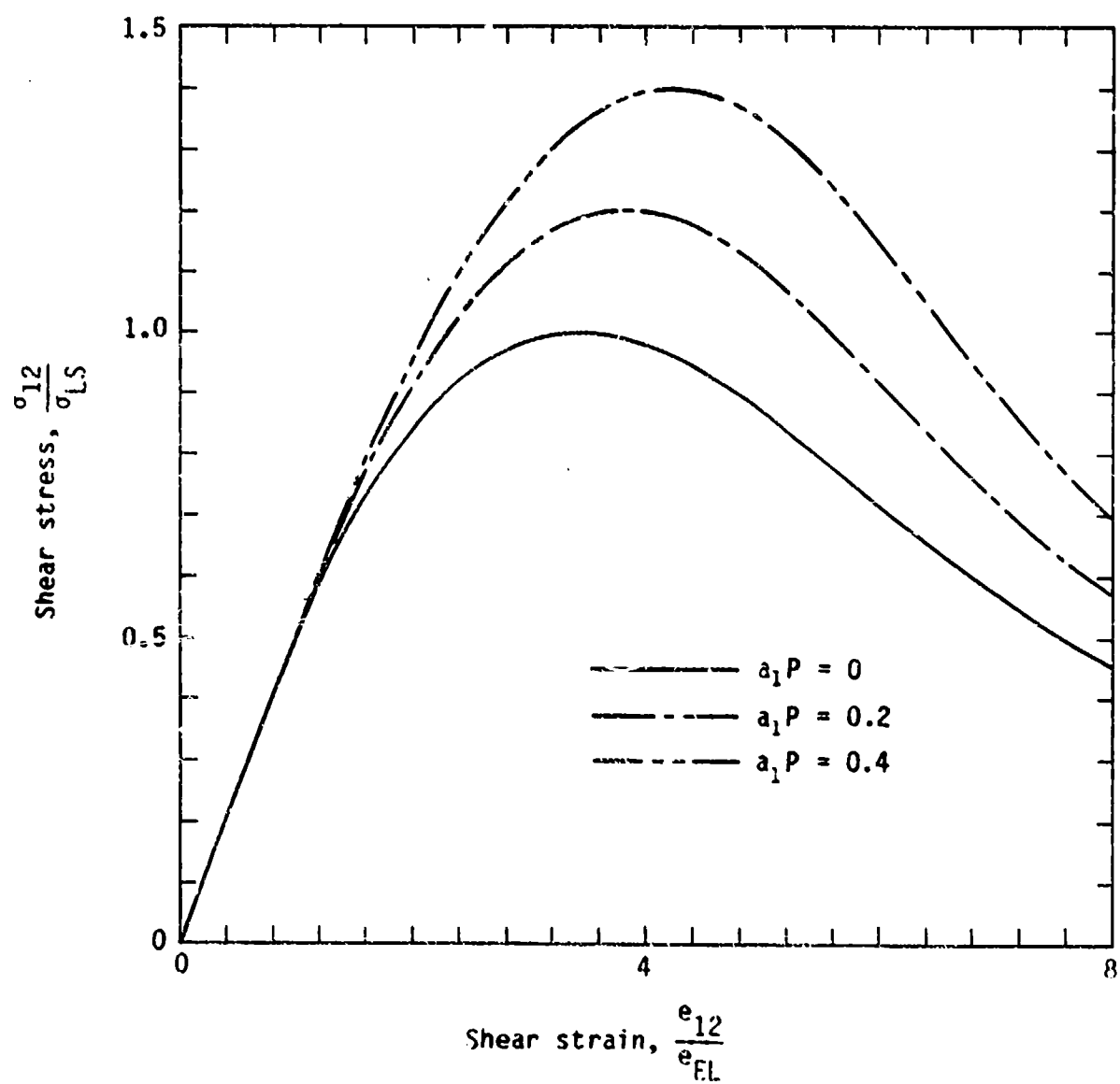


Figure 4. Effect of mean pressure on the stress-strain curve.

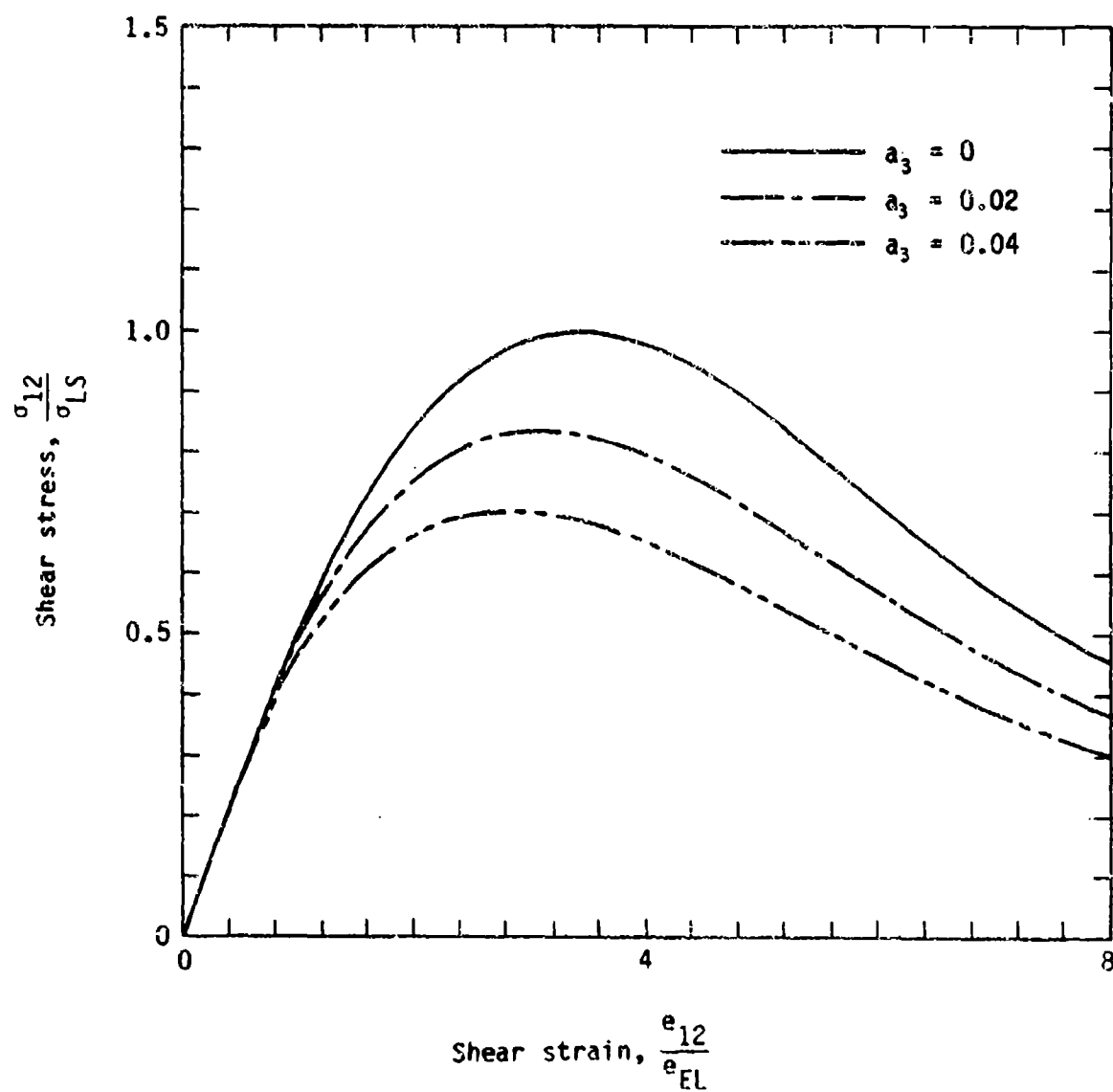


Figure 5. Effect of the parameter  $a_3$ , or the invariant of strain gradient, on stress-strain response.

stress at the limit state,  $\sigma_{LS}$ , and strain has been normalized with respect to the strain at the elastic limit,  $e_{EL}$ . The other material and control parameters used in the numerical investigations were assigned the values:

$$\begin{aligned} L_0 &= 50 \sqrt{3} & L_p &= 100 \sqrt{3} & a_2 &= 0.1 & \sigma_{LS} &= 1 & \bar{g}^i &= 10 \\ a_4 &= 10 \sqrt{3} & \frac{E}{2(1+\nu)} &= 2 & \bar{e}_L^i &= 10 & e_{EL} &= 25 & P &= 100 \\ \epsilon &= 10^{-4} & \sigma_{LS} &= 100 \sqrt{3} & \Delta e_{12} &= 0.5 \end{aligned}$$

Figure 2 shows the effect of the parameter  $n$  in the hardening regime for  $a_1 = 0$ ,  $a_3 = 0$ , and  $a_5 = 1$ . Note that the curve is smoother with a smaller value for  $n$ .

Figure 3 shows the effect of the parameter  $a_5$  in the softening regime for  $a_1 = 0$ ,  $a_3 = 0$ , and  $n = 0.5$ . By changing the values of  $a_5$ , different postpeak behaviors can be simulated. As a limiting case, the material is perfectly plastic when  $a_5$  is equal to zero.

Figure 4 illustrates the effect of mean pressure on the stress-strain curve for  $a_1 = 0$ ,  $a_5 = 0.5$ , and  $n = 0.5$ . As shown in the figure, the strength of the material increases with an increase in mean pressure.

The effect of the strain gradient on the stress-strain curve is shown in Figure 5 for  $a_1 = 0$ ,  $a_5 = 0.5$  and  $n = 0.5$ . One of the assumptions used in the current model is displayed in this figure, i.e., the stress is a function of both strain and strain gradient. The strength of the material is reduced with an increase in strain gradient.

To conclude this section, Figure 6 shows the loading, unloading, and reloading of the model by changing the sign of  $\Delta e_{12}$  for  $a_1 = 0$ ,  $a_3 = 0$ ,  $a_5 = 0.5$  and  $n = 0.5$ .

The above figures show that the current model can represent many response features that are typical for geological materials (Refs. 1, 3, and 7). If larger values of  $\Delta e_{12}$  are used, the response becomes less smooth, but the essential features are retained.

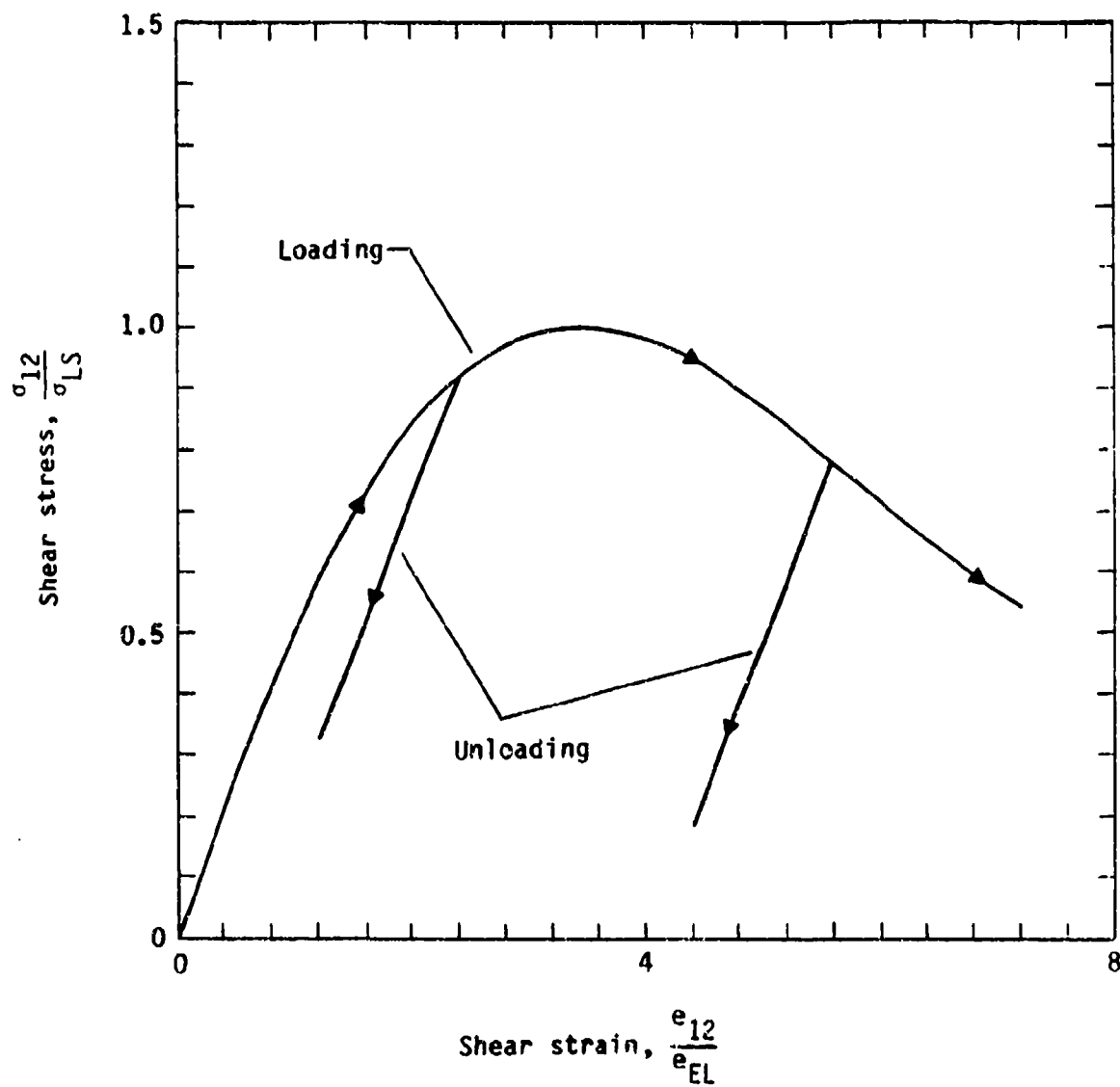


Figure 6. Illustrations of loading, unloading, and reloading in the hardening and softening regimes.

#### IV. COMPARISONS WITH OTHER NUMERICAL DATA

##### DYNAMIC RESPONSE OF THE INTERFACE UNDER SHEAR

The constitutive relation for a material point in soil has been established. In order to obtain the global response of the soil-concrete interface under dynamic shear loading, the finite element method (Ref. 15) together with a time integrator (Ref. 16) can be used. These two discretization processes provide approximate solutions of complex problems for which analytical solutions might not be available.

In this section, finite element approximations over a given geometrical domain are described first. Then, the field variable is discretized in the time domain by using a Newmark integrator in time.

For the soil-concrete interface shown in Figure 1, the notations of engineering shear stress ( $\tau$ ) and strain ( $\gamma$ ) are used for convenience. It is assumed that  $\tau = \sigma_{12}$ , and that the displacement ( $u$ ) is a function of ( $x$ ) only, and in a unique direction, perpendicular to ( $x$ ).

With these assumptions, it follows that

$$\gamma = u_{,x} \quad (24)$$

and the one-dimensional wave equation for shear is given as

$$\tau_{,x} = \rho u_{,tt} \quad (25)$$

where  $\rho$  is the mass density.

In the elastic regime, stress is related to the displacement through the relation:

$$\tau = G\gamma = \frac{E}{2(1 + \nu)} u_{,x} \quad (26)$$

Plasticity theory is used to determine stress in the hardening and softening regimes.

For the soil bar of length (L), the variational formulation of Eq. 25 is

$$\int_0^L (\tau_{,x} - \rho u_{,tt}) w \, dx = 0 \quad \text{for all } w \quad (27)$$

where  $w$  is the test or weighting function. After performing an integration by parts, it follows that

$$\int_0^L w_{,x} \tau \, dx + \int_0^L \rho w u_{,tt} \, dx = \frac{f_L}{A} w_L + \frac{f_0}{A} w_0 \quad \text{for all } w \quad (28)$$

where  $f_L$  and  $f_0$  are the external loads applied on the ends of the soil bar,  $x = L$ , and  $x = 0$ , respectively.

Divide the soil bar into elements of equal length ( $h$ ) as shown in Figure 7 and use linear element shape functions  $\psi_i$ , i.e.,

$$\psi_1 = 1 - \eta \quad (29)$$

$$\psi_2 = \eta \quad (30)$$

where

$$\eta = \frac{x - x_i}{h} \quad (31)$$

Then the integrals in Eq. 28 can be converted to a sum with the result that

$$\sum_{e=1}^N \left( h \int_0^1 \rho^e w^e u_{,tt}^e \, d\eta + \int_0^1 w_{,n}^e \tau^e \, d\eta \right) = \frac{f_L}{A} w_L + \frac{f_0}{A} w_0 \quad (32)$$

for all  $w$ , where  $N$  is the number of elements and  $\rho^e$  is the element mass density. The global functions  $u_{,tt}$ ,  $\tau$ ,  $w$ , and  $w_{,x}$  are computed element by element in the domain of the problem  $0 \leq x \leq L$ . In an arbitrary element ( $e$ ), these functions are interpolated as follows:



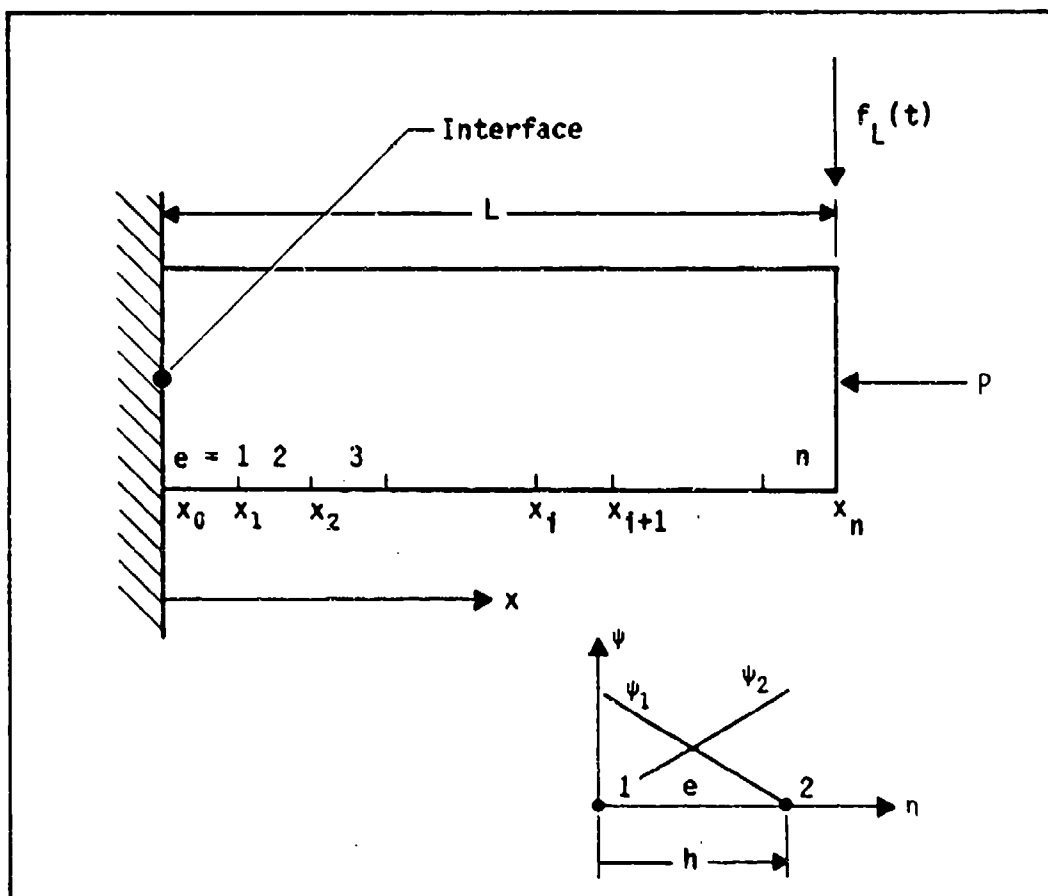


Figure 7. Finite element mesh of the soil bar and the shape function used.

$$u_{,tt}^e = u_{,tt}^{e1} \psi_1 + u_{,tt}^{e2} \psi_2 \quad (33)$$

$$\tau^e = \tau^{e1} \psi_1 + \tau^{e2} \psi_2 \quad (34)$$

$$w^e = w^{e1} \psi_1 + w^{e2} \psi_2 \quad (35)$$

$$w_{,n}^e = w_{,n}^{e1} \psi_{1,n} + w_{,n}^{e2} \psi_{2,n} \quad (36)$$

where the superscript e1 denotes the left node of each element, and e2, the right node.

If the consistent element mass matrix is defined to be

$$M_{ij}^e = \rho^e h \int_0^1 \psi_i \psi_j \, d\eta \quad (37)$$

and the element internal force vector is

$$f_i^{Ie} = \int_0^1 \psi_{i,n} \tau^e \, d\eta \quad (38)$$

then, an alternate form of Eq. 32 is

$$\sum_{e=1}^N \left( \sum_{i,j=1}^2 w^{ei} M_{ij}^e u_{,tt}^{ej} + \sum_{i=1}^2 f_i^{Ie} w^{ei} \right) = \frac{f_L}{A} w_L + \frac{f_0}{A} w_0 \quad (39)$$

for all  $w$ .

Now relate the global nodal values,  $w_k$ ,  $u_{k,tt}$ , and the element nodal or local values,  $w^{ei}$ ,  $u_{,tt}^{ei}$ , as follows:

$$w_k = w^{(k-1)2} = w^{k1} \quad (40)$$

$$u_{k,tt} = u_{,tt}^{(k-1)2} = u_{,tt}^{k1} \quad (41)$$

where the subscript  $k$  refers to the node number, and the two superscripts denote the element number and the element node number, respectively. Assume  $\rho$  is constant for each element. Then, with  $M_{ij}$  representing the global mass

matrix and  $f_i$ , the global force vector, the variational formulation of the equation of motion can be written in indicial notation as

$$M_{ij} u_{j,tt} = f_i \quad (42)$$

where

$$[M_{ij}] = \rho h \begin{bmatrix} 1/3 & 1/6 & 0 & 0 & 0 & 0 \\ 1/6 & 2/3 & 1/6 & 0 & 0 & 0 \\ 0 & 1/6 & 0 & 0 & 0 & 0 \\ 0 & 0 & 0 & \ddots & \ddots & 0 \\ \vdots & \vdots & \vdots & \vdots & \vdots & \vdots \\ 0 & 0 & 0 & \ddots & \ddots & 1/3 \end{bmatrix} \quad (43)$$

and

$$\{f_i\} = \left\{ \begin{array}{c} \frac{f_0}{A} + \tau^{11} \\ - \left( \tau^{12} + \tau^{21} \right) \\ - \left( \tau^{22} + \tau^{31} \right) \\ \vdots \\ \frac{f_L}{A} + \tau^{n2} \end{array} \right\} \quad (44)$$

Equation 42 represents a set of ordinary differential equations defined in the time domain. The global force vector is the sum of the external force and internal force vectors, through which the constitutive equation sub-routine is used. To solve this set of equations, a time integrator is used. To make the system explicit in time, a diagonal mass matrix is required. The diagonal mass matrix is constructed by summing each row of the global mass matrix as shown in Eq. 43, and putting the sum of each row into the corresponding diagonal position. Although the time step must be chosen according to the stability condition, no matrix storage is required, and calculations using the explicit method are much simpler than those using the implicit method.

Introduce the discrete values of time,

$$t^n = ns \quad \text{for a fixed time step } s \quad (45)$$

where the superscript  $n$  is an integer denoting the discrete time, and let  $u_i^n$ ,  $v_i^n$ , and  $a_i^n$  be approximations to displacement  $u_i(t^n)$ , velocity  $v_i(t^n)$ , and acceleration  $u_{i,tt}(t^n)$  at node  $i$  respectively. A particular form of the Newmark integrator is

$$u_i^{n+1} = u_i^n + s v_i^n + \frac{s^2}{2} a_i^n \quad (46)$$

$$v_i^{n+1} = v_i^n + s \left[ (1 - \alpha) a_i^n + \alpha a_i^{n+1} \right] \quad (47)$$

To introduce numerical damping, a value of  $\alpha = 0.8$  was used. In addition, Eq. 42 is approximated with the equation

$$M_{ij} a_j^{n+1} = f_i^{n+1} \quad (48)$$

Hence, for given initial and boundary conditions, the field variable  $u_i$  at each node can be found without determining the tangent stiffness matrix. With the use of the constitutive subroutine mentioned earlier, the algorithm for obtaining the dynamic response of the soil is as follows:

Step 1--Input material constants and control parameters.

Step 2--Input initial and boundary conditions.

Step 3--Start time integration with time step ( $s$ ):

$$t^n = t^{n-1} + s$$

Step 4--Calculate displacements at each node ( $i$ ):

$$u_i^n = u_i^{n-1} + s v_i^{n-1} + \frac{s^2}{2} a_i^{n-1} \quad i = 1, 2, \dots, nn$$

and replace  $u_1$  at the end of the soil bar by the given boundary condition.

Step 5--Find total strains and strain increments at each element (i) by using

$$\gamma_i^n = \frac{u_{i+1}^n - u_i^n}{h} \quad i = 1, 2, \dots, nn - 1$$

and

$$\Delta \gamma_i^n = \gamma_i^n - \gamma_i^{n-1}$$

Step 6--Compute inelastic strain gradients at each element (i) according to the following relation:

$$(\bar{g}_i^n)^n = \frac{(\gamma_{i+1}^i)^n - (\gamma_i^i)^n}{h} \quad i = 1, 2, \dots, N-1$$

Step 7--Call constitutive subroutine to get the stresses  $(\tau_i^n)$ .

Step 8--Calculate the force vector at each node (i) by means of Eq. 44.

Step 9--Calculate accelerations at each node:

$$a_i^n = \frac{1}{m_{ij}} f_i^n$$

where  $m_{ij}$  is the diagonal element of the diagonal mass matrix.

Step 10--Calculate the velocity vector:

$$v_i^n = v_i^{n-1} + s \left[ (1 - \alpha) a_i^{n-1} + \alpha a_i^n \right]$$

Step 11--If the results  $\tau(x,t)$  and  $\gamma(x,t)$  are needed--print out, then go to Step 3.

To verify the current approach, comparisons with other existing data were required. Existing experimental data, however, do not show the relation

between the size of the localization zone and the applied load. An alternate theoretical approach (Ref. 12) with a nonlocal continuum, called an imbricate continuum, illustrates numerically the dynamic response of a one-dimensional bar subjected to tensile waves. Two tensile waves are initiated at the ends of the bar, then the waves meet together at the middle point. That point will be the first to go into the postpeak regime. Other material points of the bar near the middle point will also get into the postpeak regime because of the nonlocal approach. Thus, the strain softening accompanied by localization can be simulated. In the imbricate continuum model, a bilinear stress-strain relation is adopted. Although the problem of the soil-concrete interface seems to be different from that in Reference 12, the basic features are the same in both cases if the middle point of the one-dimensional bar is changed to a rigid constraint, and only half the bar length is considered. Therefore, the numerical solutions of Reference 12 can be used to corroborate the interface model by taking the concrete part as a rigid body and applying the current constitutive model to the soil part, as shown in Figure 7.

By dividing the soil bar of length ( $L = 1$ ) into 20 elements, using the time step  $\Delta t = 0.2 h \sqrt{\rho/G}$ , and assigning to the other parameters the following values:

$$\begin{aligned} \bar{\epsilon}_L^i &= 0.16 & \epsilon &= 10^{-4} & \sigma_{LS} &= \sqrt{3} \\ a_1 &= 0 & a_2 &= 0.1 & a_3 &= 0.08 \\ a_4 &= 0.1 \sqrt{3} & a_5 &= 0.6 & n &= 0.4 \end{aligned}$$

an approximate solution is obtained. Results are shown in Figures 8 to 19.

For purely elastic behavior, Figure 8 shows the propagation of the stress wave at various times for

$$\begin{aligned} G &= \frac{E}{2(1 + \nu)} = 1 & \rho &= 1 & f_L &= 0.4 H[t] \\ L_0 &= 0.9 \sqrt{3} & L_p &= \sqrt{3} \end{aligned}$$

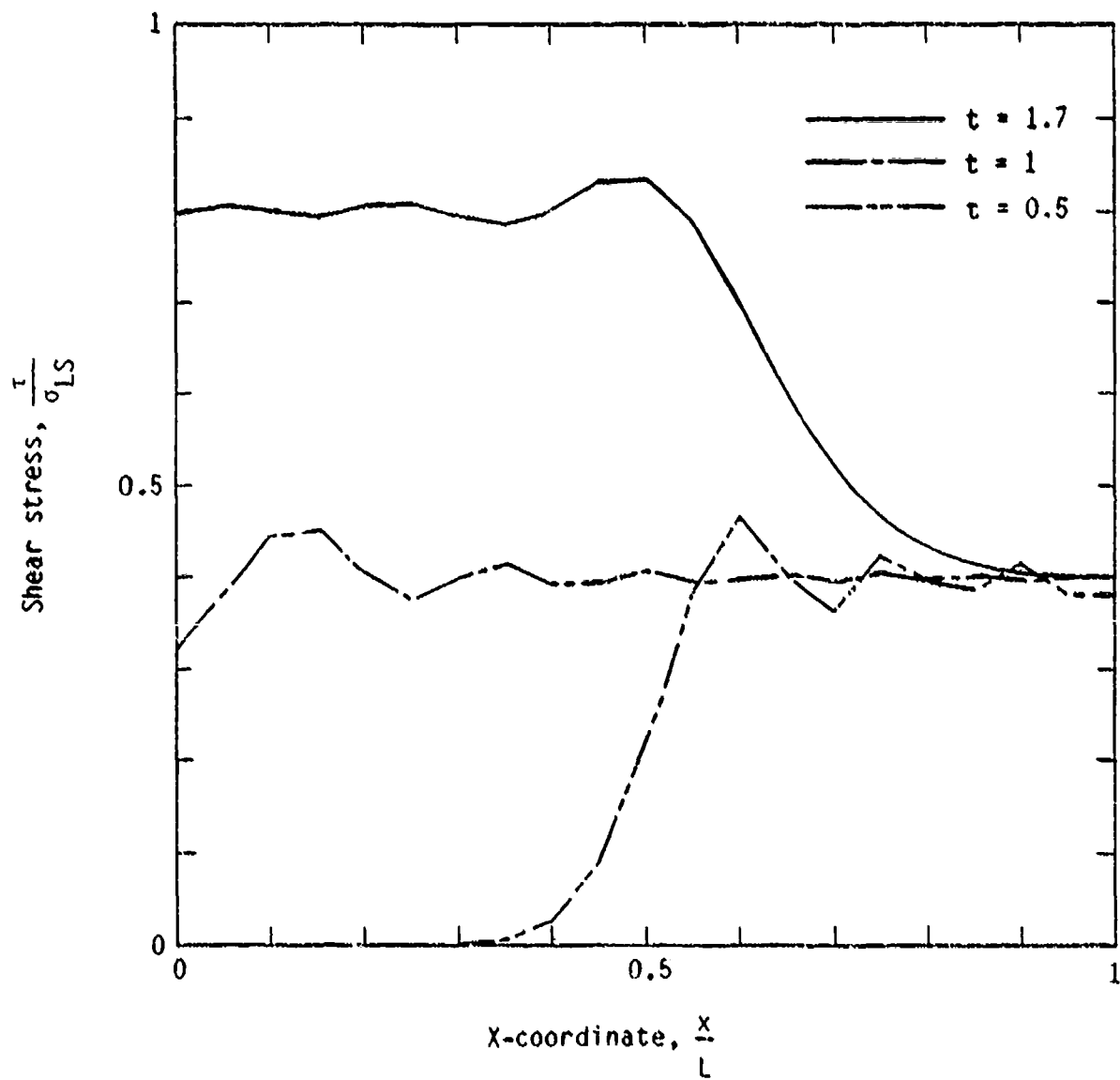


Figure 8. Illustration of elastic stress wave at various times.

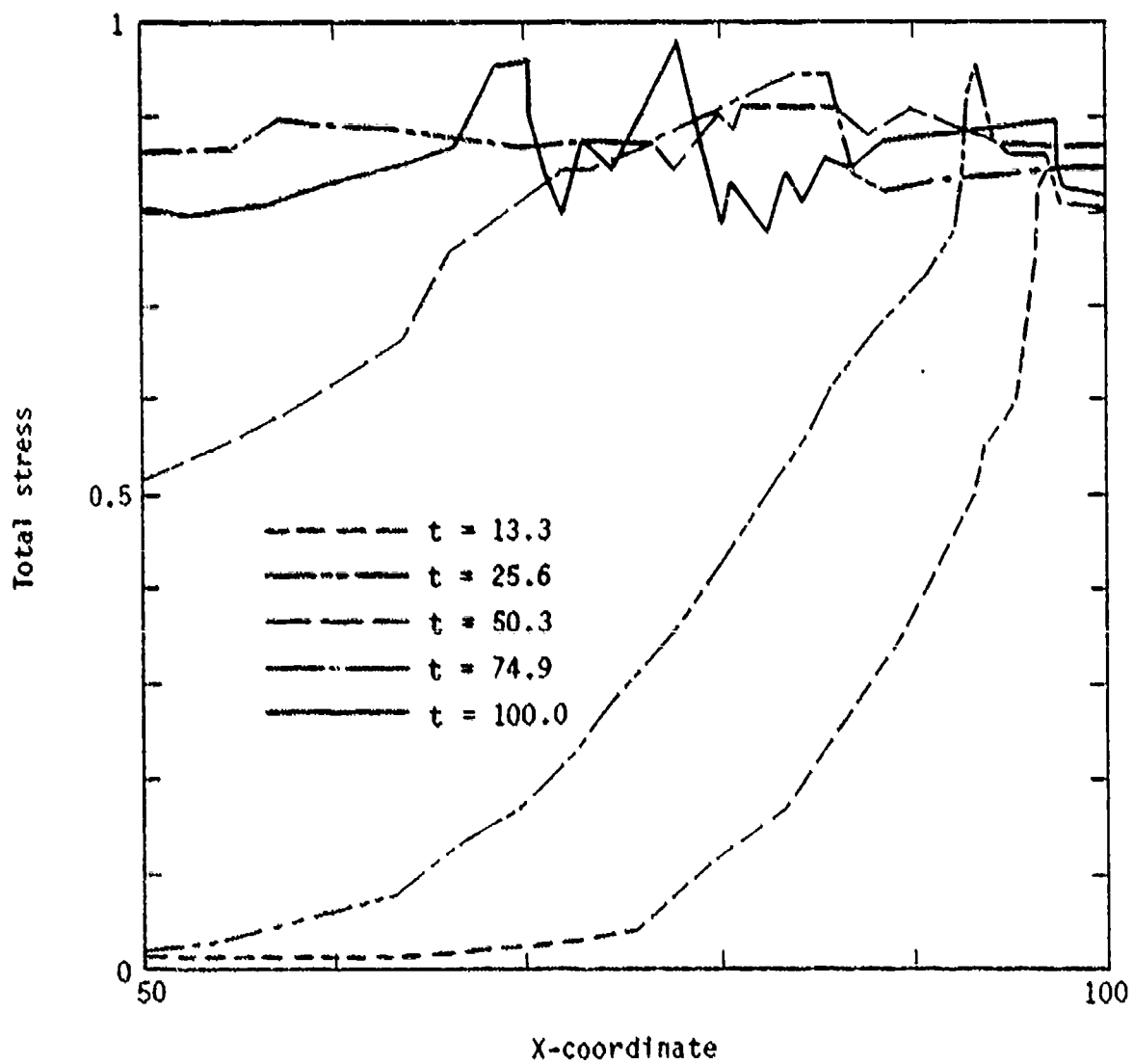


Figure 9. Spatial distribution of stress at various times (from Ref. 12).



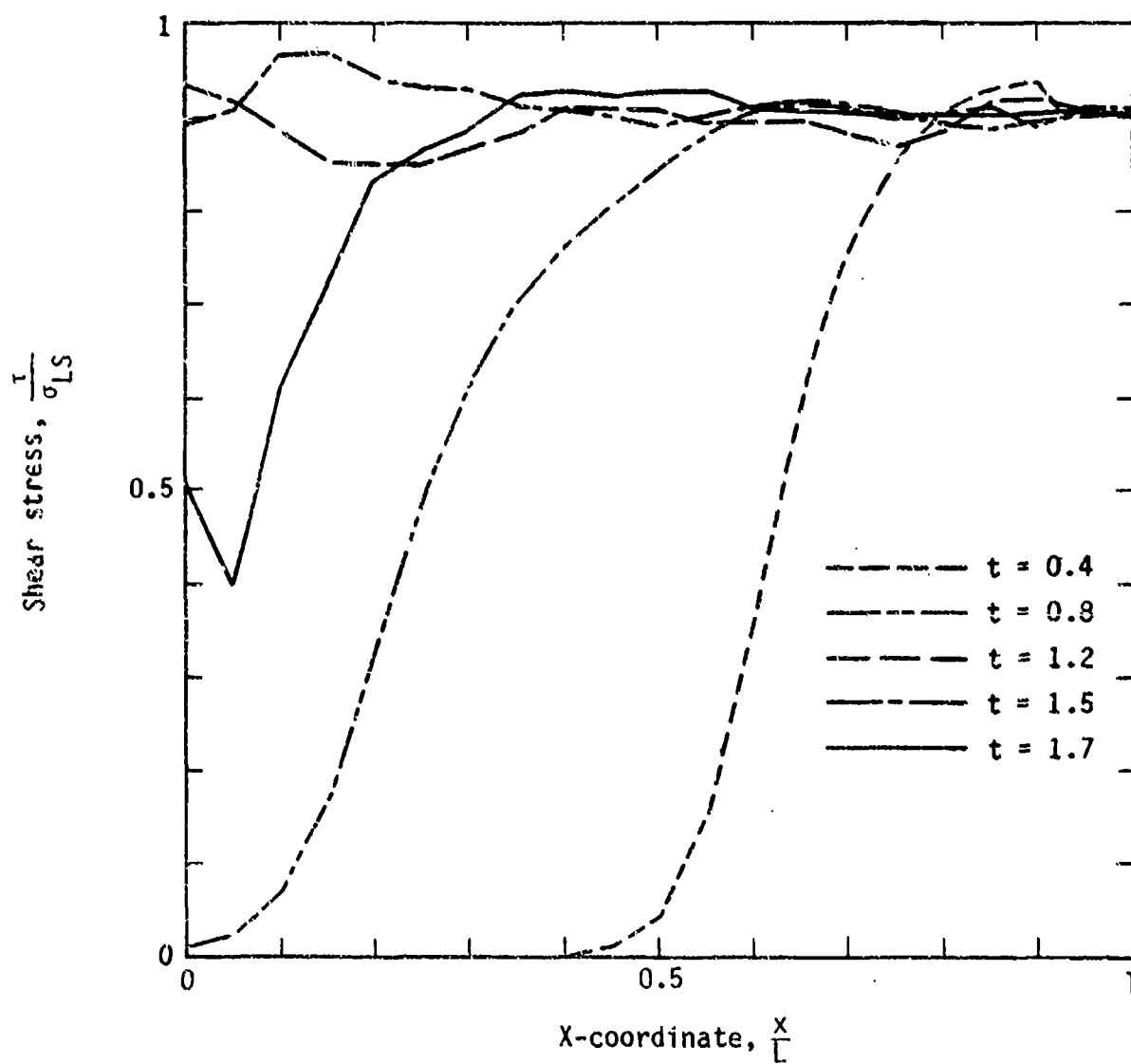


Figure 10. Spatial distribution of stress at various times using the current approach.

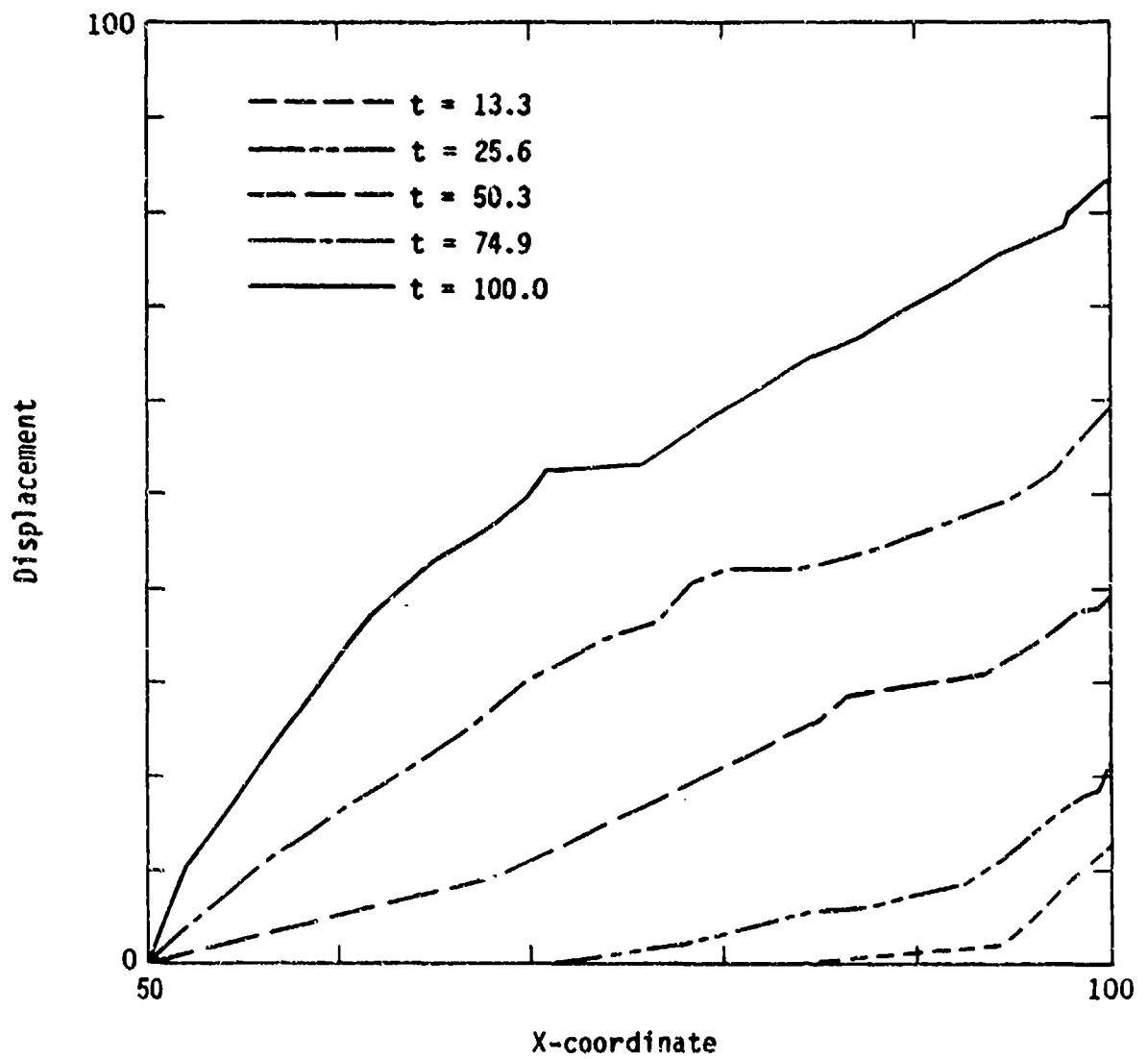


Figure 11. Spatial distributions of displacement field at various times (from Ref. 12).

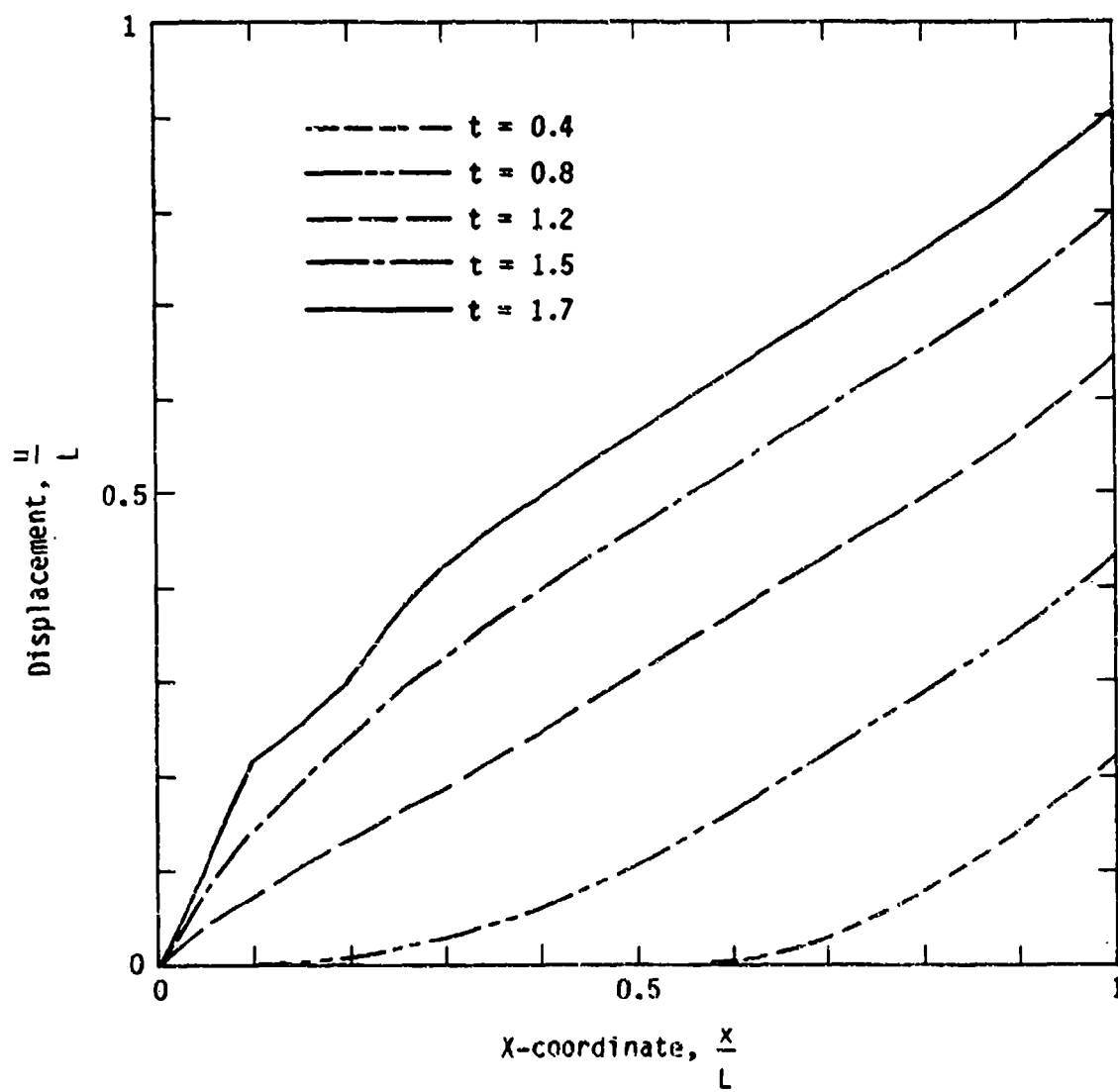


Figure 12. Spatial distribution of displacement field at various times using the current approach.

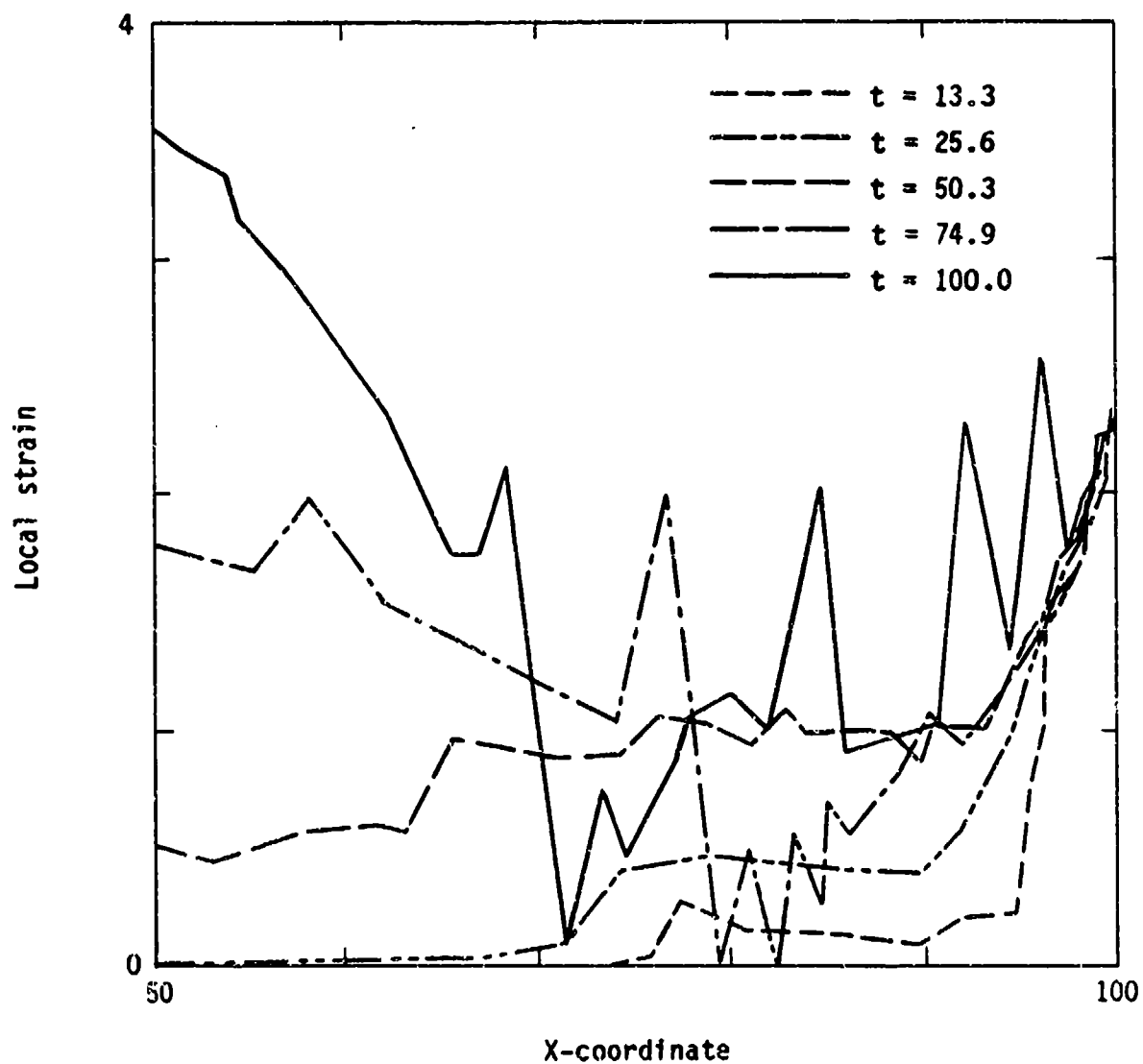


Figure 13. Spatial distribution of strain at various times (from Ref. 12).

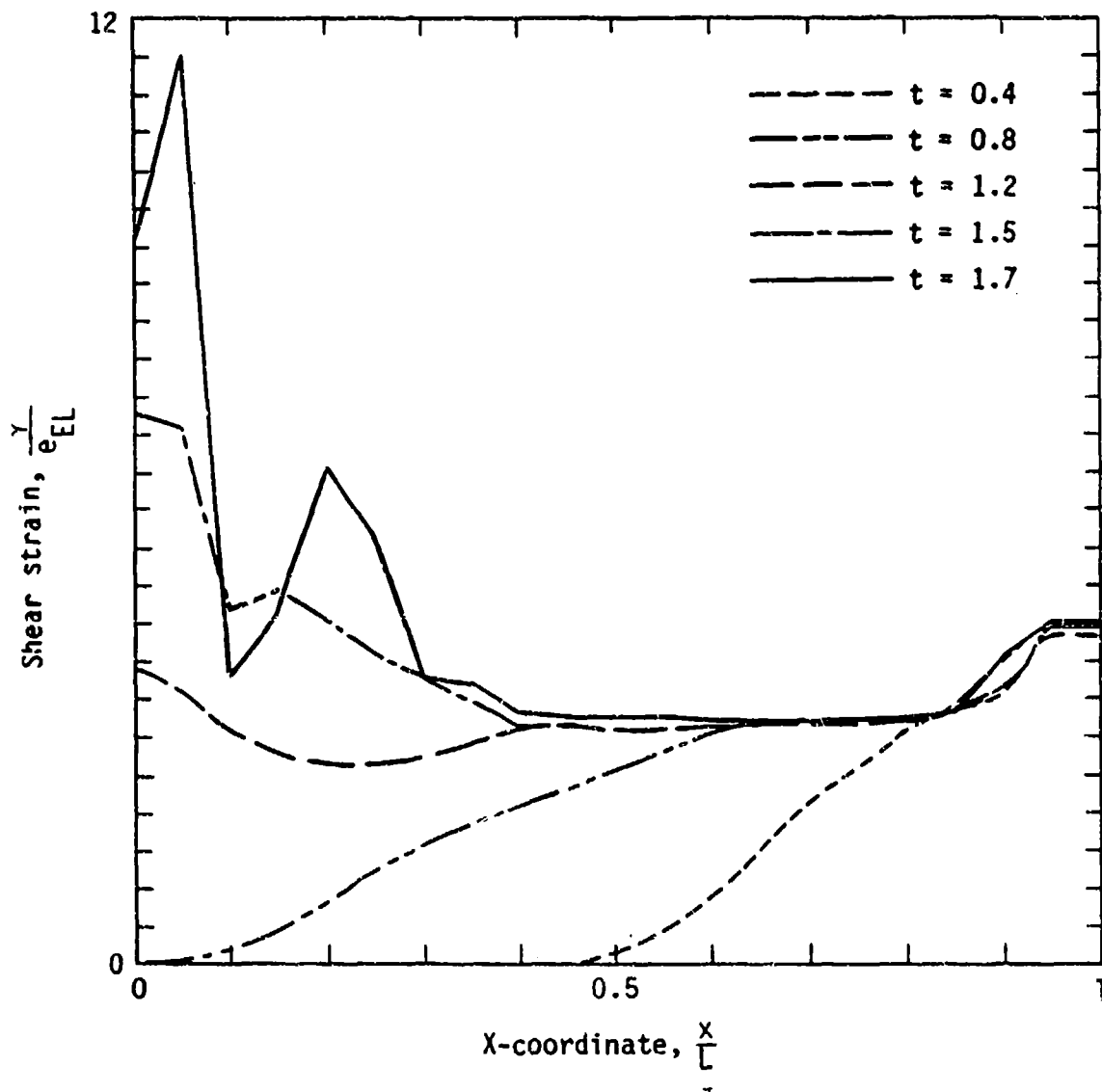


Figure 14. Spatial distribution of strain at various times using the current approach.

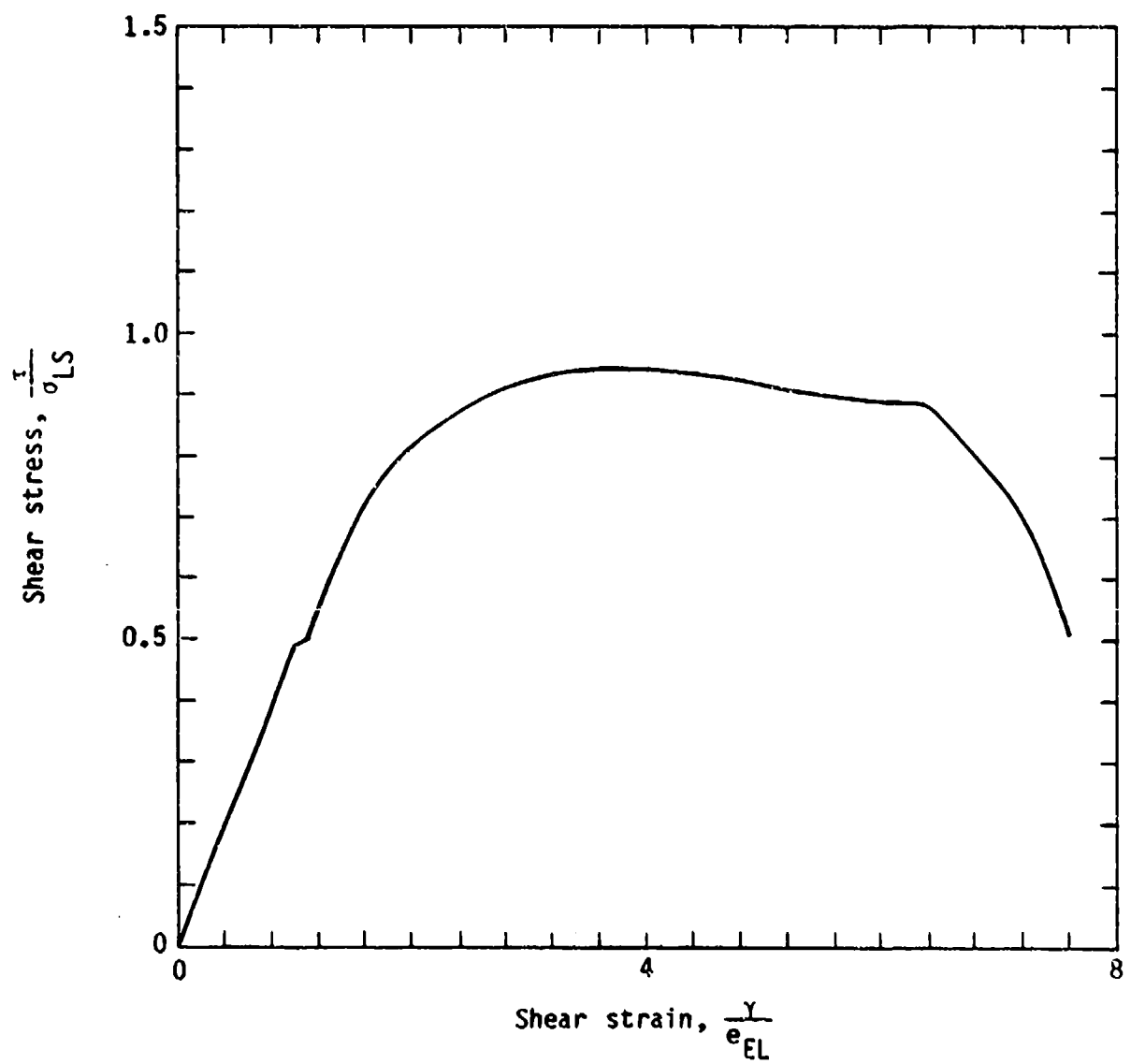


Figure 15. Shear stress-strain path for element 1 at time  $t = 1.7$ .

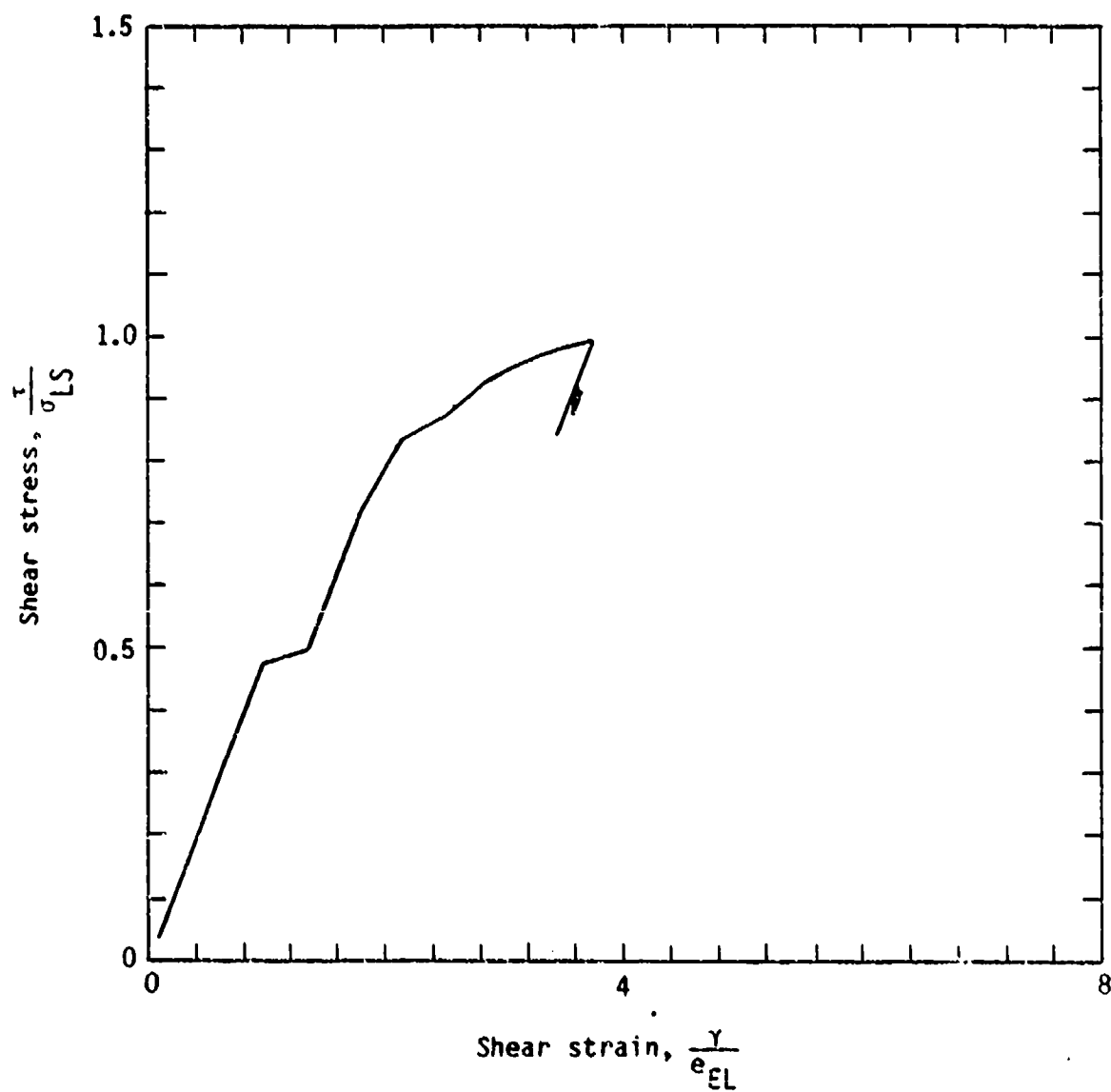


Figure 16. Shear stress-strain path for element 20 at time  $t = 1.7$ .

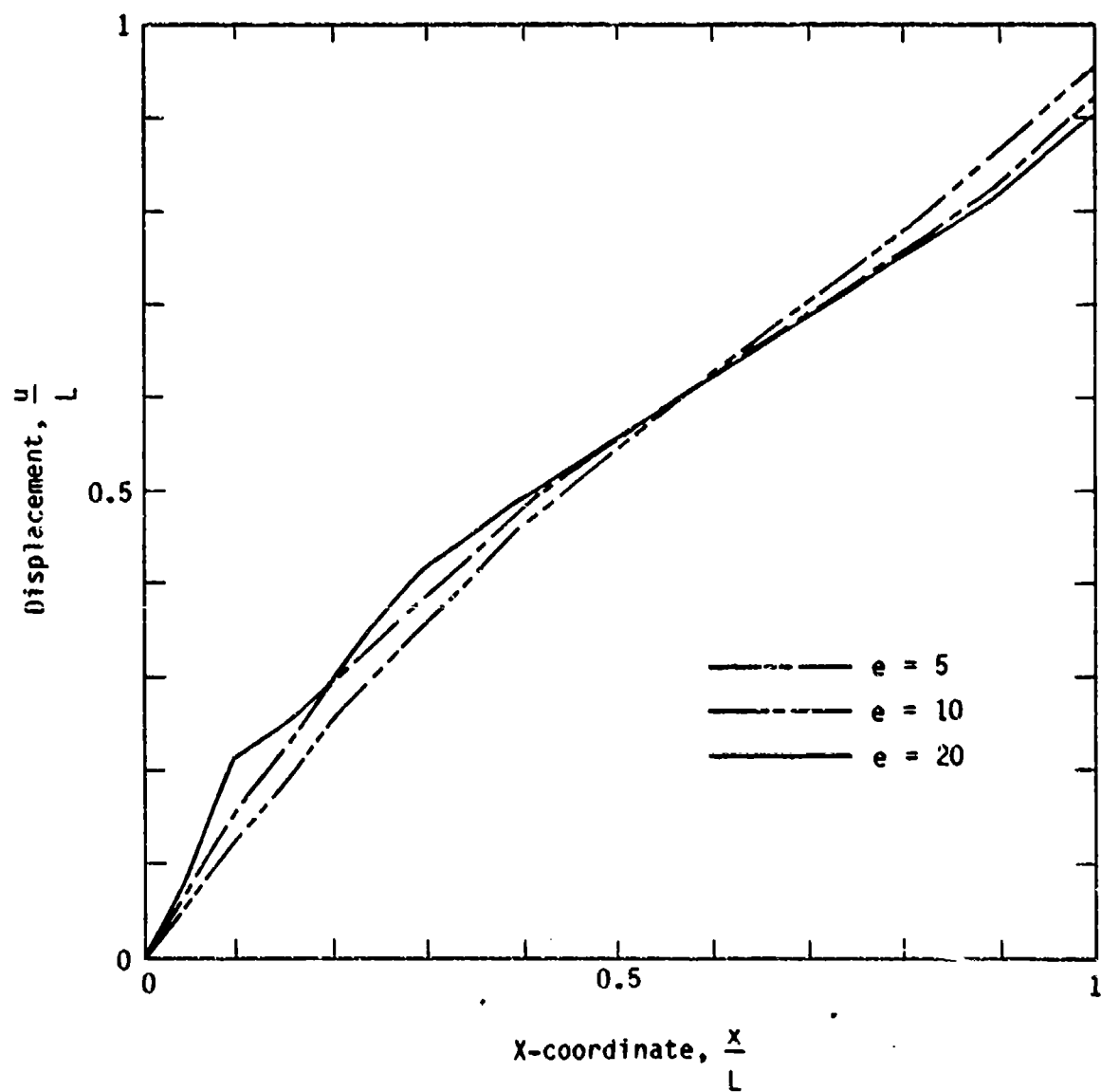


Figure 17. Distribution of displacement at  $t = 1.7$  for different meshes.



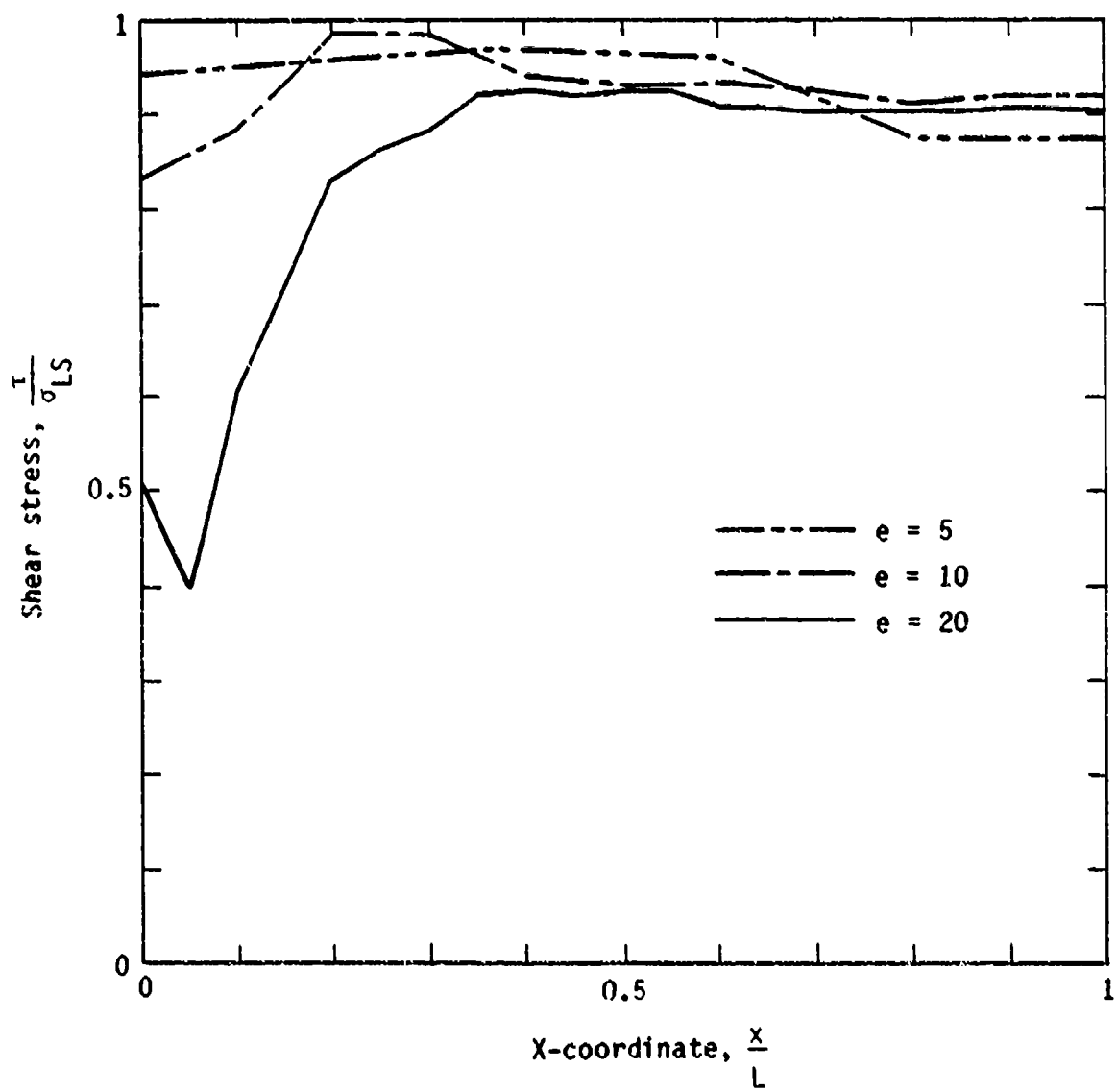


Figure 18. Distribution of stress at  $t = 1.7$  for different meshes.

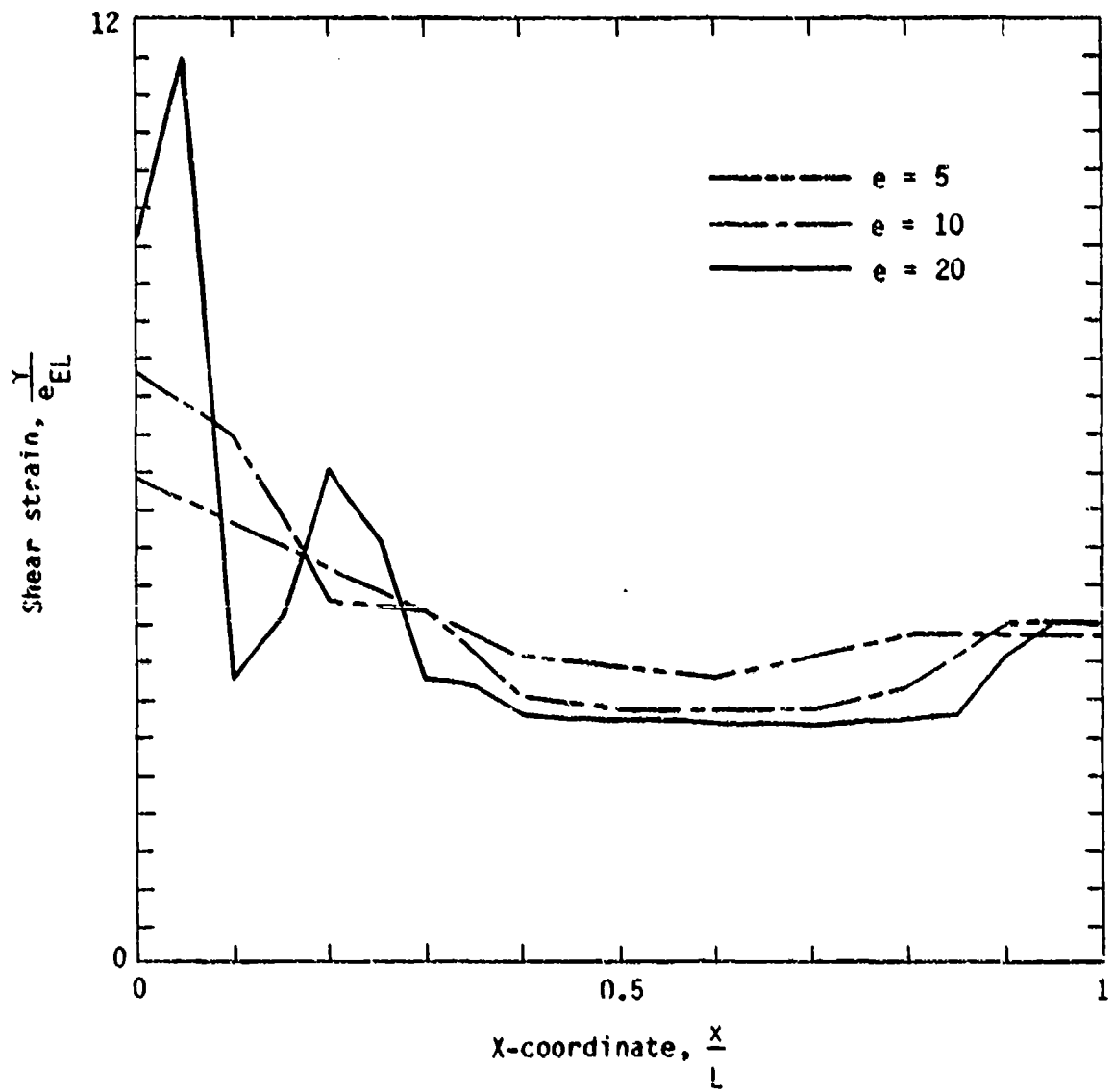


Figure 19. Distribution of strain at  $t = 1.7$  for different meshes.

The material parameters ( $G$  and  $\rho$ ) are chosen so that the wave speed equals unity. Except for numerical dispersion and dissipation, the approximate solution is a reasonable representation of the exact shear wave.

Figures 9 to 14 show the inelastic solutions and the one-to-one comparisons with numerical solutions of Reference 12 for

$$G = \frac{E}{2(1 + \nu)} = 2 \quad \rho = 2 \quad f_L = 0.9 H[t]$$

$$L_0 = 0.5 \sqrt{3} \quad L_p = \sqrt{3}$$

From these figures, it is apparent that the tendencies of the dynamic responses of the two problems are alike, but with the simpler computational approach given by the current model. When the shear wave, which propagates from the right end of the soil bar, reaches the interface, a reflection occurs and the stress increases to the limit state which initiates softening. As the figures show, the region next to the interface is characterized by large strain and low stress, which is believed to be representative of what occurs at an interface.

Figures 15 and 16 show the stress-strain responses at  $t = 1.7$  of element 1 and element 20, which represent points near the interface and near the free end of the soil bar. Figures 17 to 19 show the convergence of the numerical solution by using different finite element meshes.

Although there is some numerical noise in the numerical solution, the localization zone, i.e., the large deformation band with stress being reduced, can be predicted near the soil-concrete interface. In addition, it appears that good results can also be obtained by using a coarse mesh.

#### STATIC RESPONSE OF THE INTERFACE UNDER SHEAR

The global response of the soil-concrete interface under static shear loading is investigated in this final subsection. The problem geometry is shown in Figure 1. The soil bar is divided into 10 linear elements, and the

load is a monotonically increasing displacement at  $x = L$ . The shear strength of the interface is assumed to be slightly smaller than other parts of the soil bar so that the interface will initiate failure.

The algorithm used for getting the static response of the interface is outlined as follows:

Step 1--Input material constants, boundary conditions, and control parameters.

Step 2--Monotonically increase the strain in the first element, and find the corresponding increment of stress, which must be the same for every element.

Step 3--Call the constitutive equation subroutine for each element. If the results are required, print them out.

Step 4--If the interface is still in the prepeak regime, go to Step 2. Otherwise, go to Step 5.

Step 5--If the previous value of stress for any element is larger than the current peak stress corresponding to that element, go into the softening regime. Otherwise, use elastic unloading.

Step 6--Go to Step 2 for the next increment of strain in the first element.

Figures 20 to 27 show the numerical solutions for the following parameters:

$$\begin{aligned}
 L_0 &= 0.5 \sqrt{3} & L_p &= \sqrt{3} & n &= 0.5 \\
 G &= \frac{E}{2(1 + \nu)} = 2 & \bar{e}_L^i &= 0.16 & \sigma_{LS} &= \sqrt{3} \\
 \varepsilon &= 10^{-4} & a_2 &= 0.1 & a_3 &= 0.1 \\
 a_4 &= 0.1 \sqrt{3} & \Delta\gamma &= 0.05 & a_1 &= 0 \\
 a_5 &= 0.6
 \end{aligned}$$

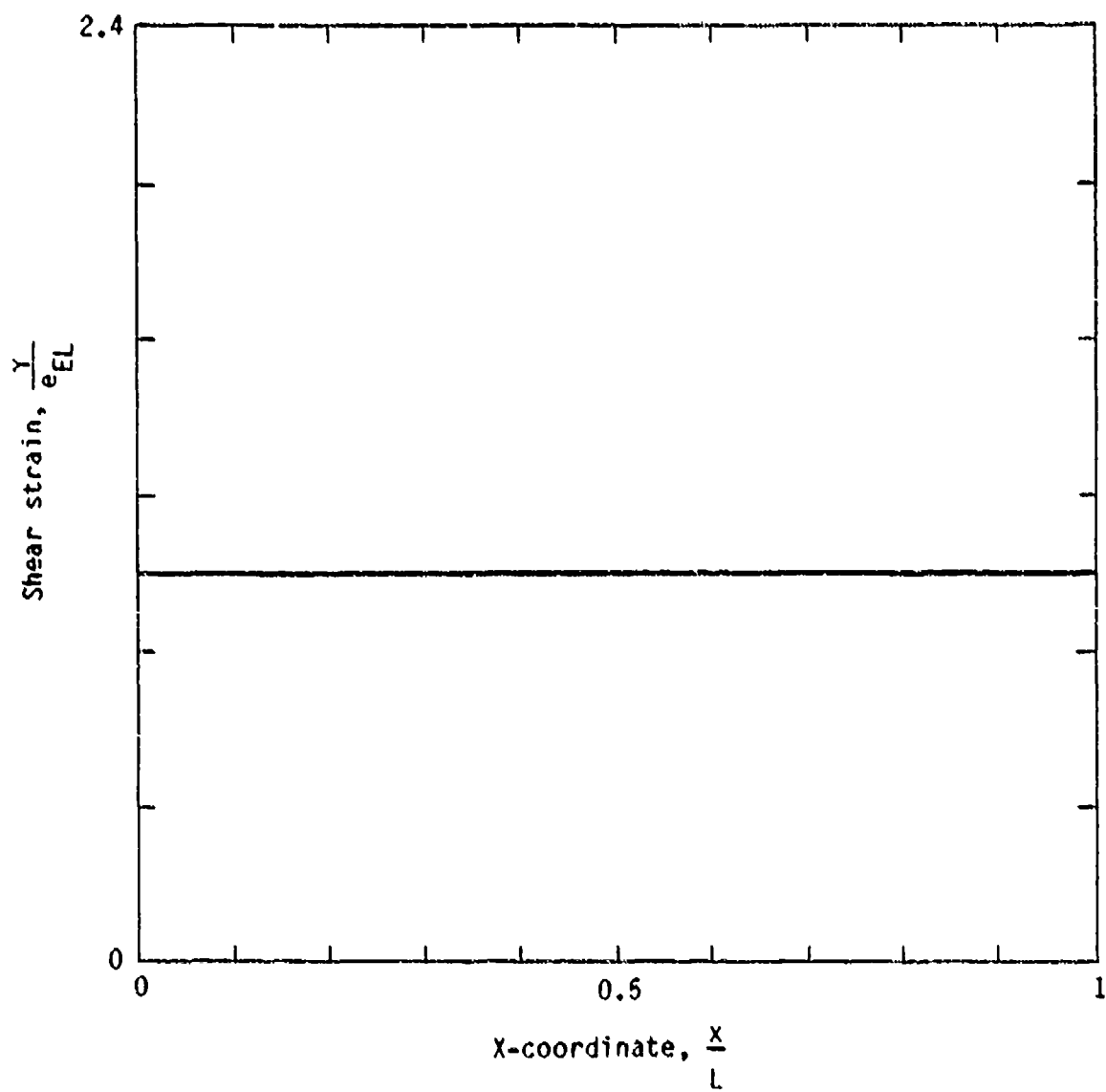


Figure 20. Strain distribution for static response in elastic regime.

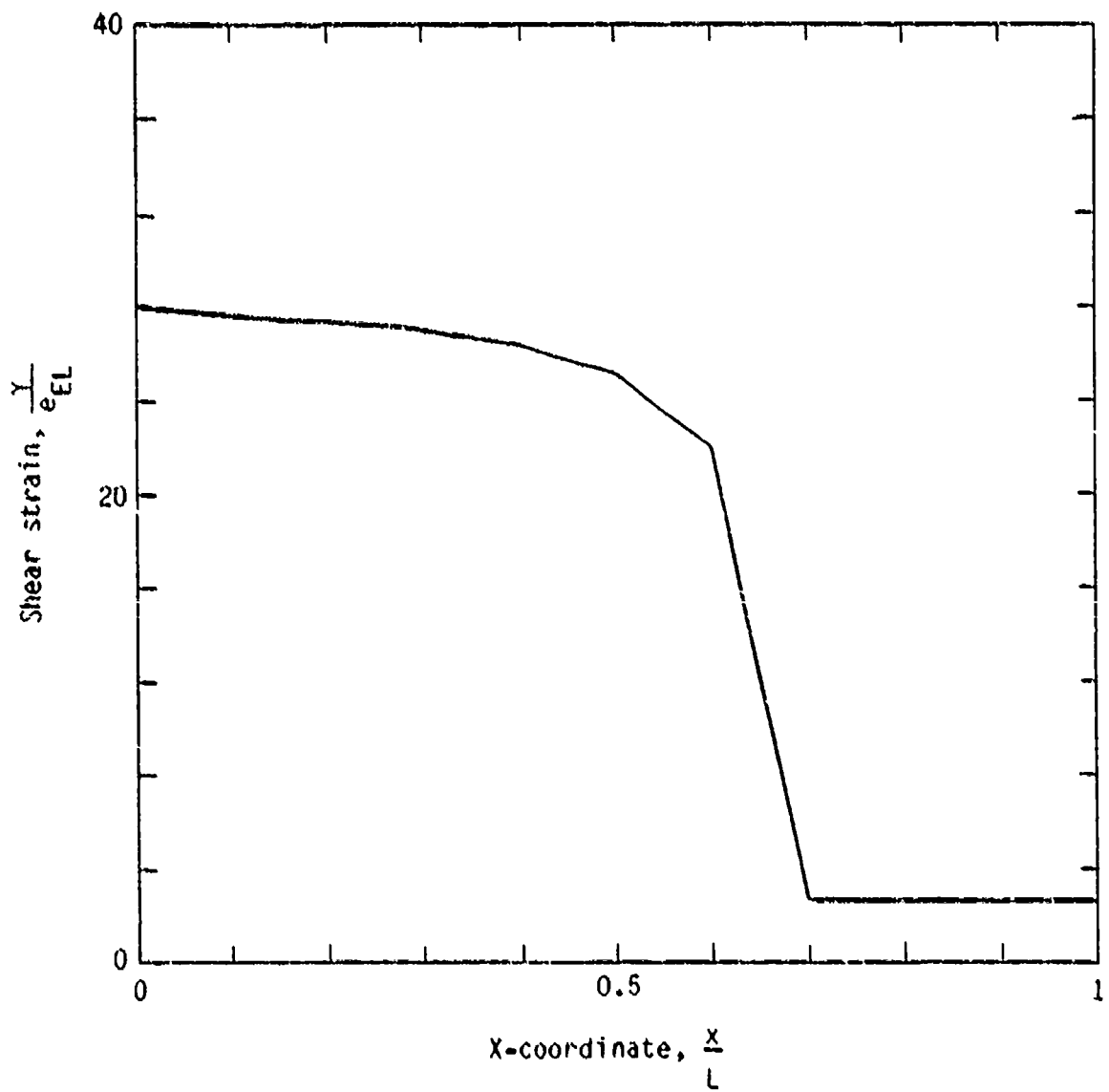


Figure 21. Strain distribution for static response in softening regime.

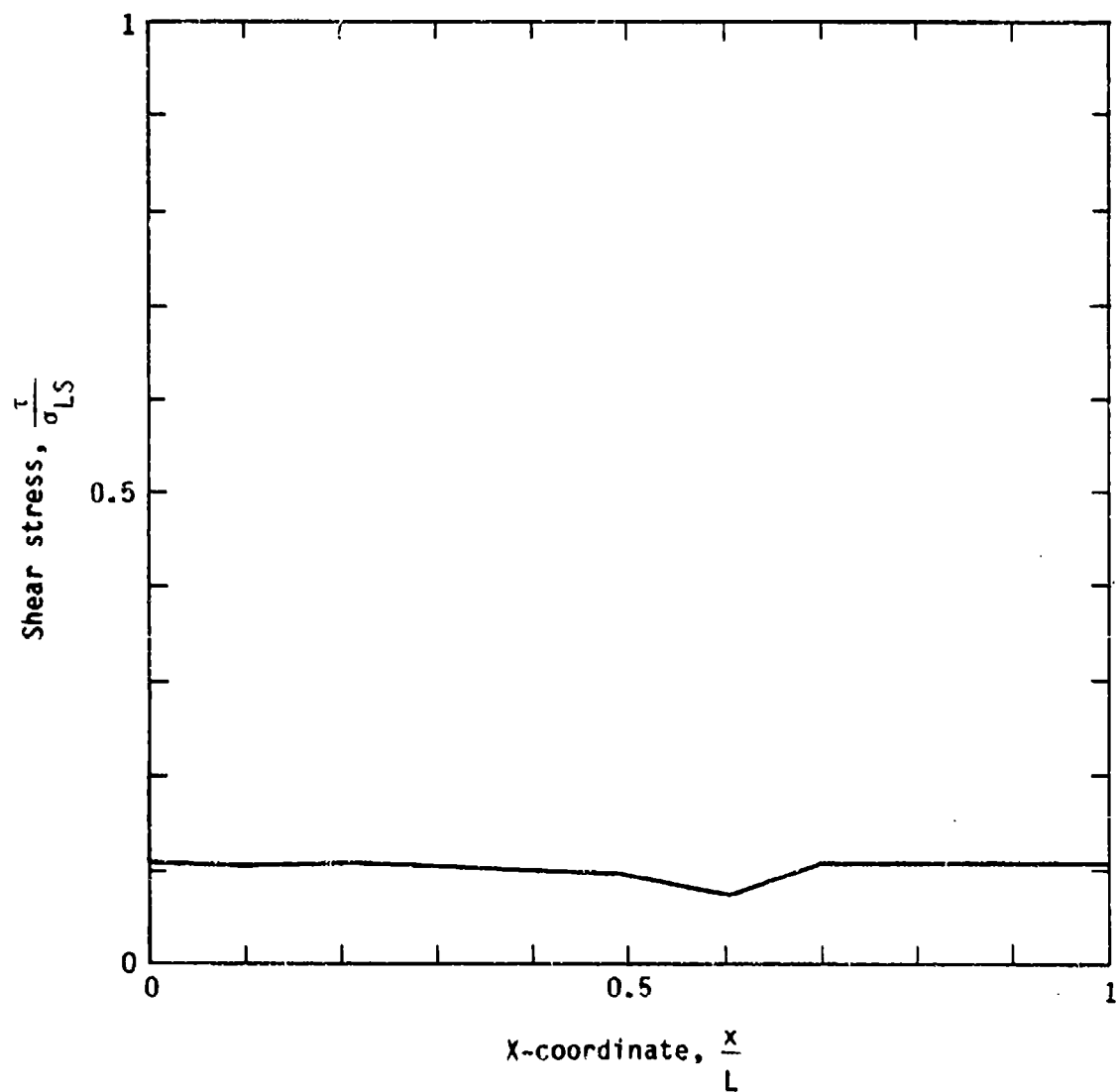


Figure 22. Stress distribution for static response in softening regime.

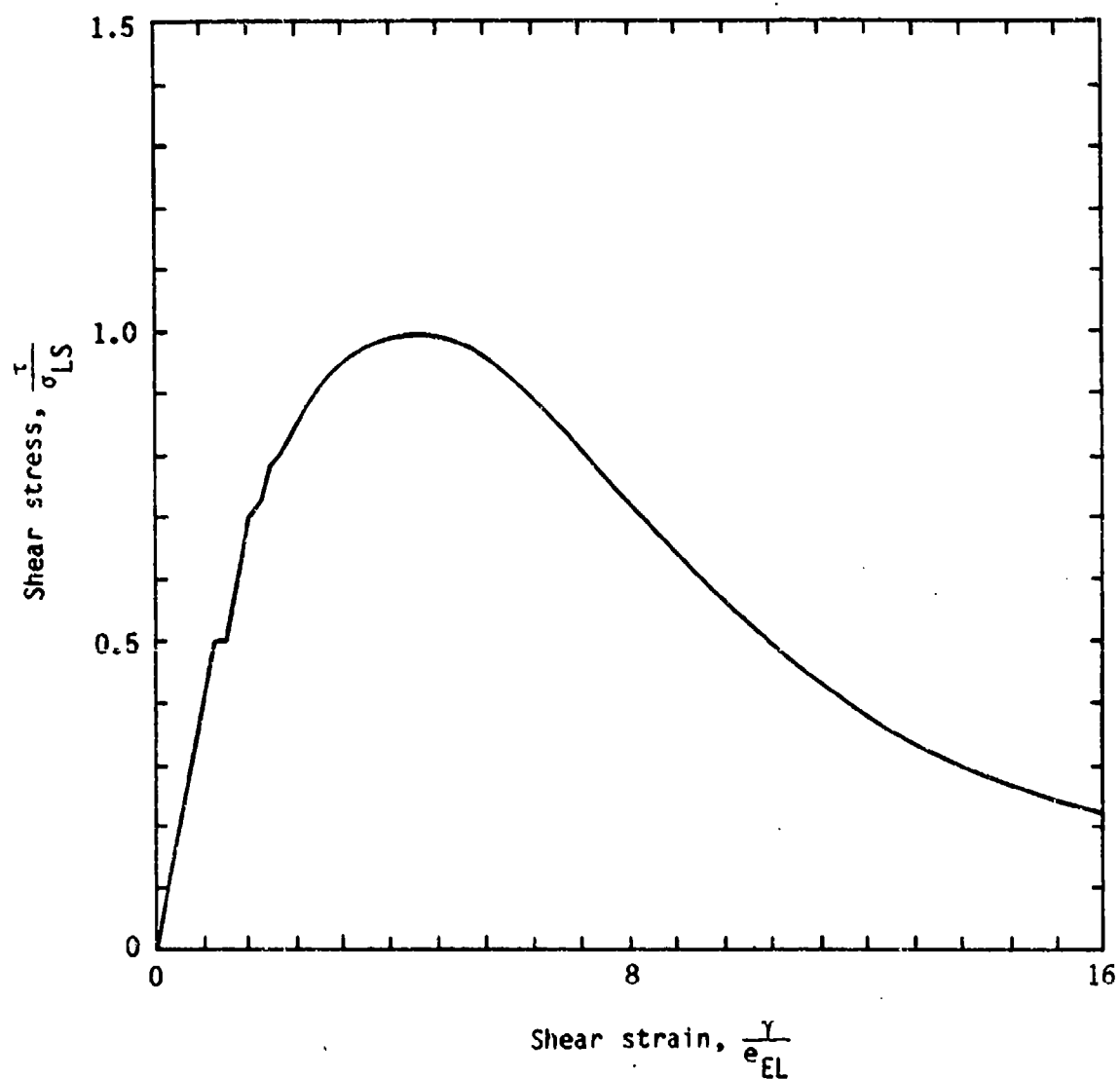


Figure 23. Shear stress-strain response of element 1.



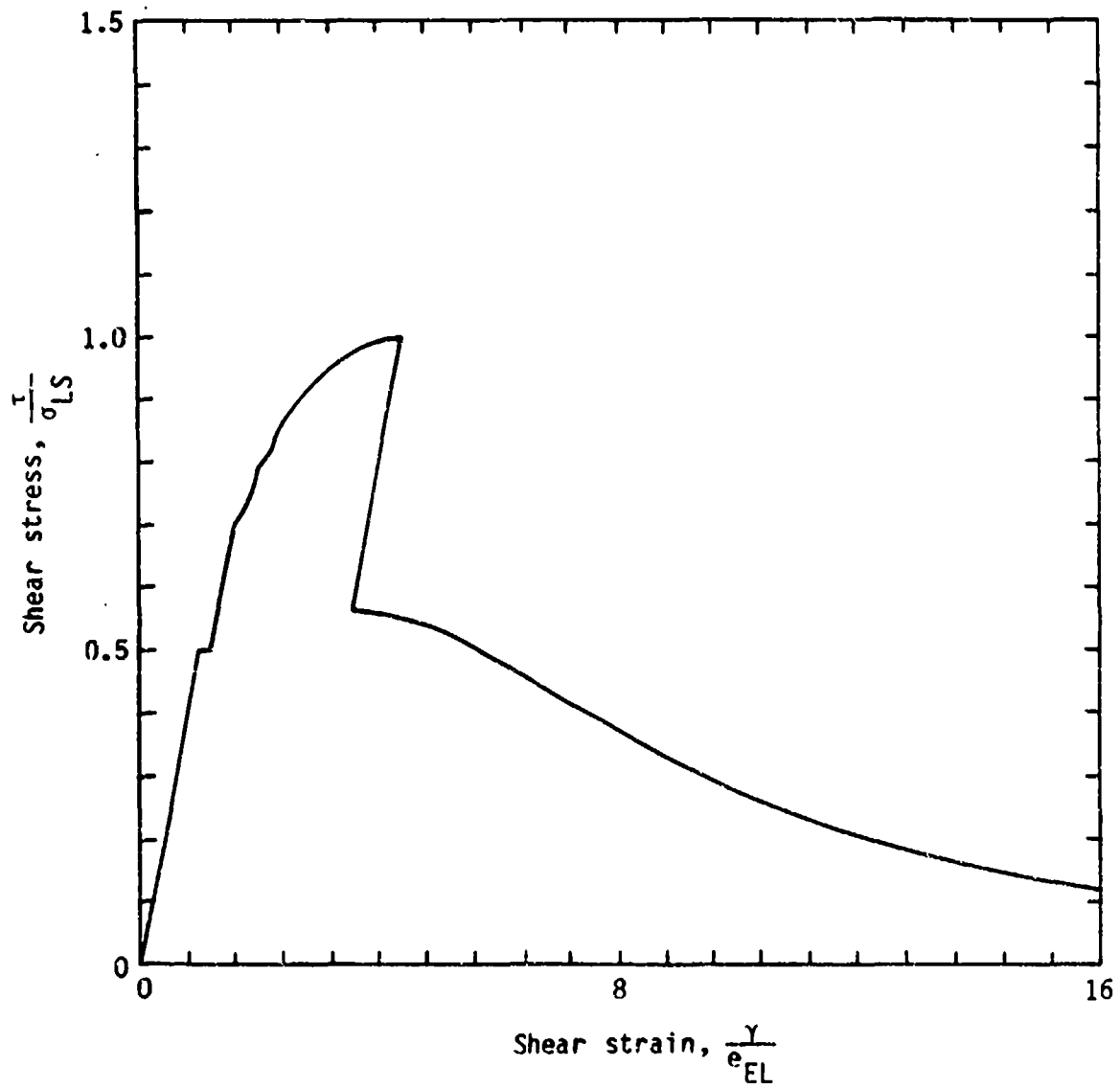


Figure 24. Shear stress-strain response of element 6.

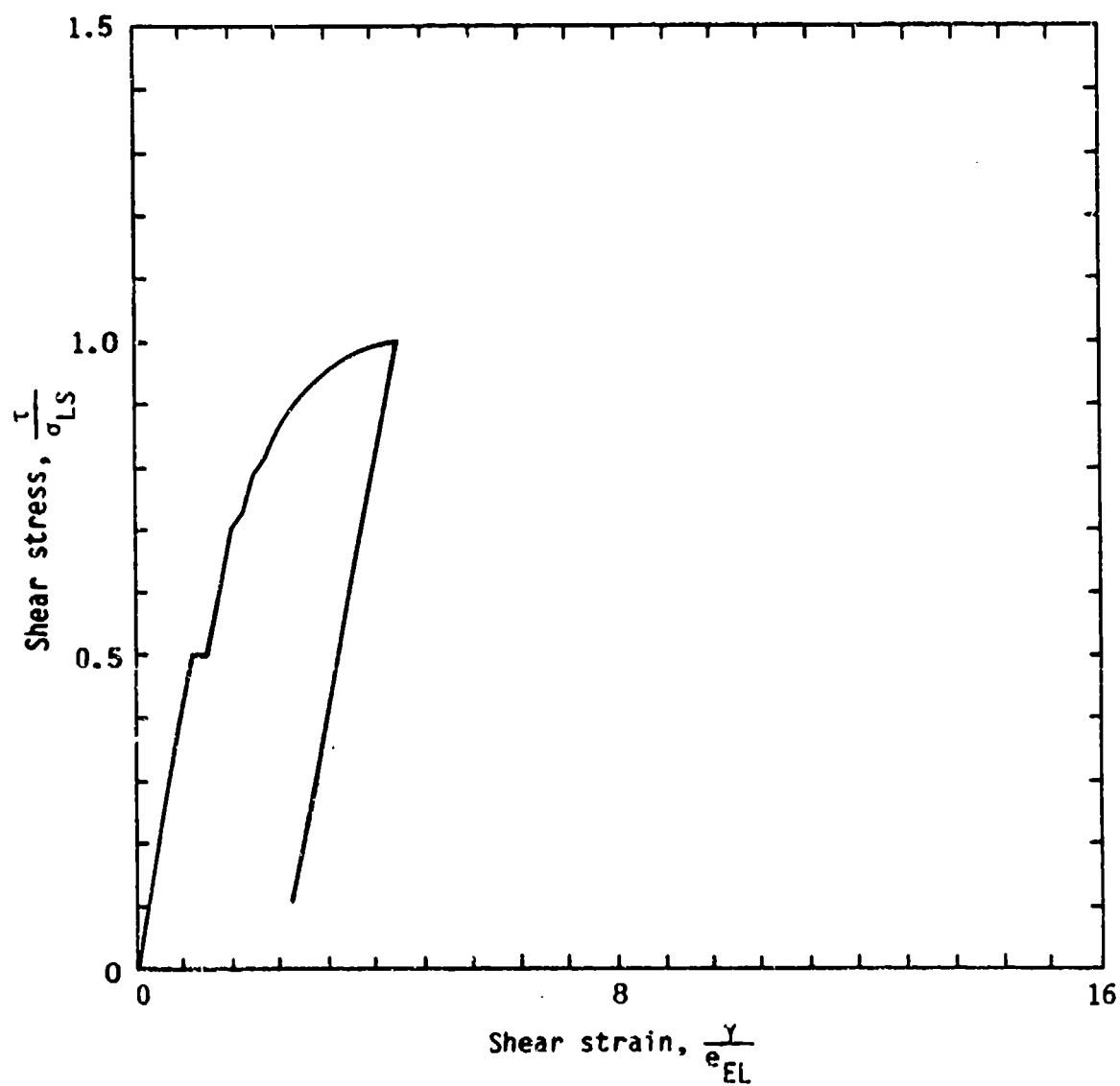


Figure 25. Shear stress-strain response of element 10.

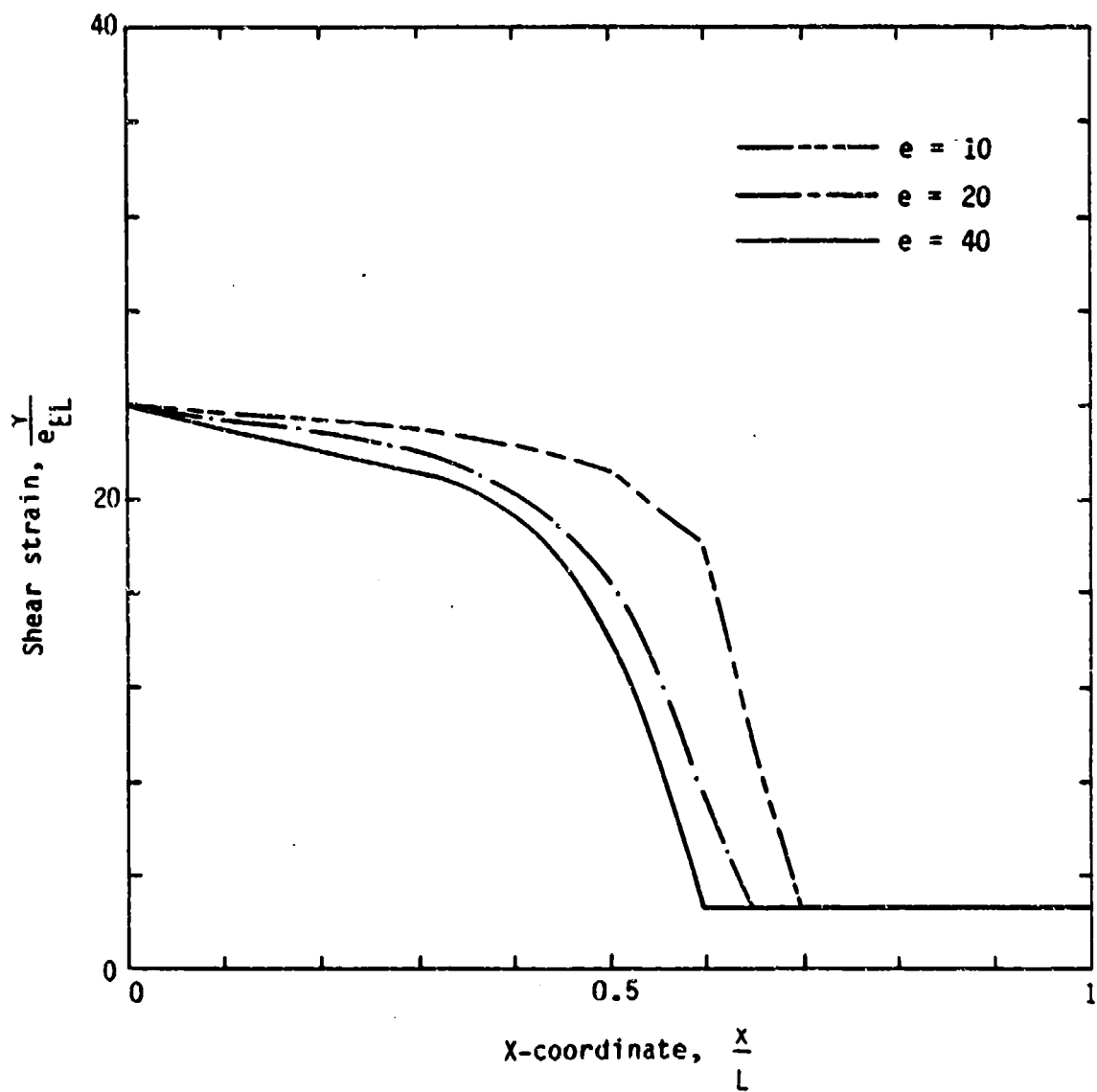


Figure 26. Strain distribution for different meshes to show convergence.

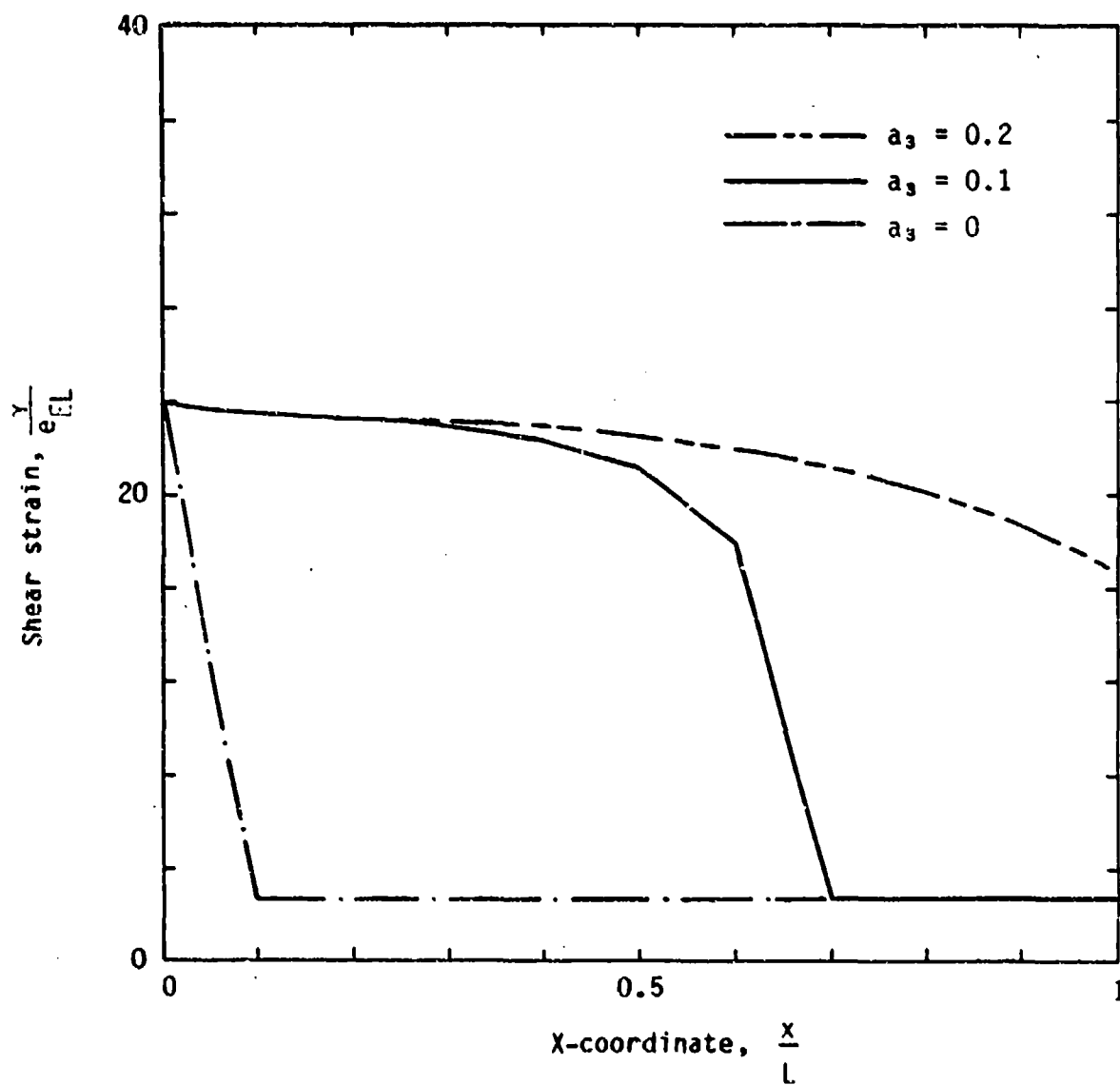


Figure 27. Effect of the parameter  $a_3$ , or the invariant of strain gradient, on the static response near the interface.

Figure 20 shows the strain distribution of static response in the elastic regime where the strain distribution is uniform. Figure 21 shows the strain distribution of the static response in the postpeak regime. Note that the strain distribution is not uniform, and that the localization zone occurs near the interface. Figure 22 shows the stress distribution that corresponds to the strain distribution of Figure 21. Since there is no distributed applied force, the stress distribution is always uniform under static loading. Figures 23 to 25 show the stress-strain responses of element 1, element 6, and element 10, respectively. Element 1 represents the region near the interface, and element 10, the opposite end of the soil bar. After the peak state, element 6 unloads elastically at first, and then goes into the softening regime. Figure 26 shows the convergence of strain distributions for different finite element meshes. Figure 27 shows the effect of strain gradients on the static response of the soil bar as reflected through various values of  $a_3$ . For  $a_3 = 0$ , i.e., local continuum approach, the localization zone cannot be predicted. This is why a classical local constitutive model cannot simulate the soil-concrete interface.

Figure 28 shows the relations between shear force and displacement under the effect of different mean pressures,  $a_1 P$ , for

$$\bar{e}_L^i = 0.4 \quad a_5 = 0.5 \quad a_3 = 0.02$$

with other parameters being unchanged. According to experimental results reported by Drumm and Desai (Ref. 3), basic features of the static response near the interface are simulated with this approach.

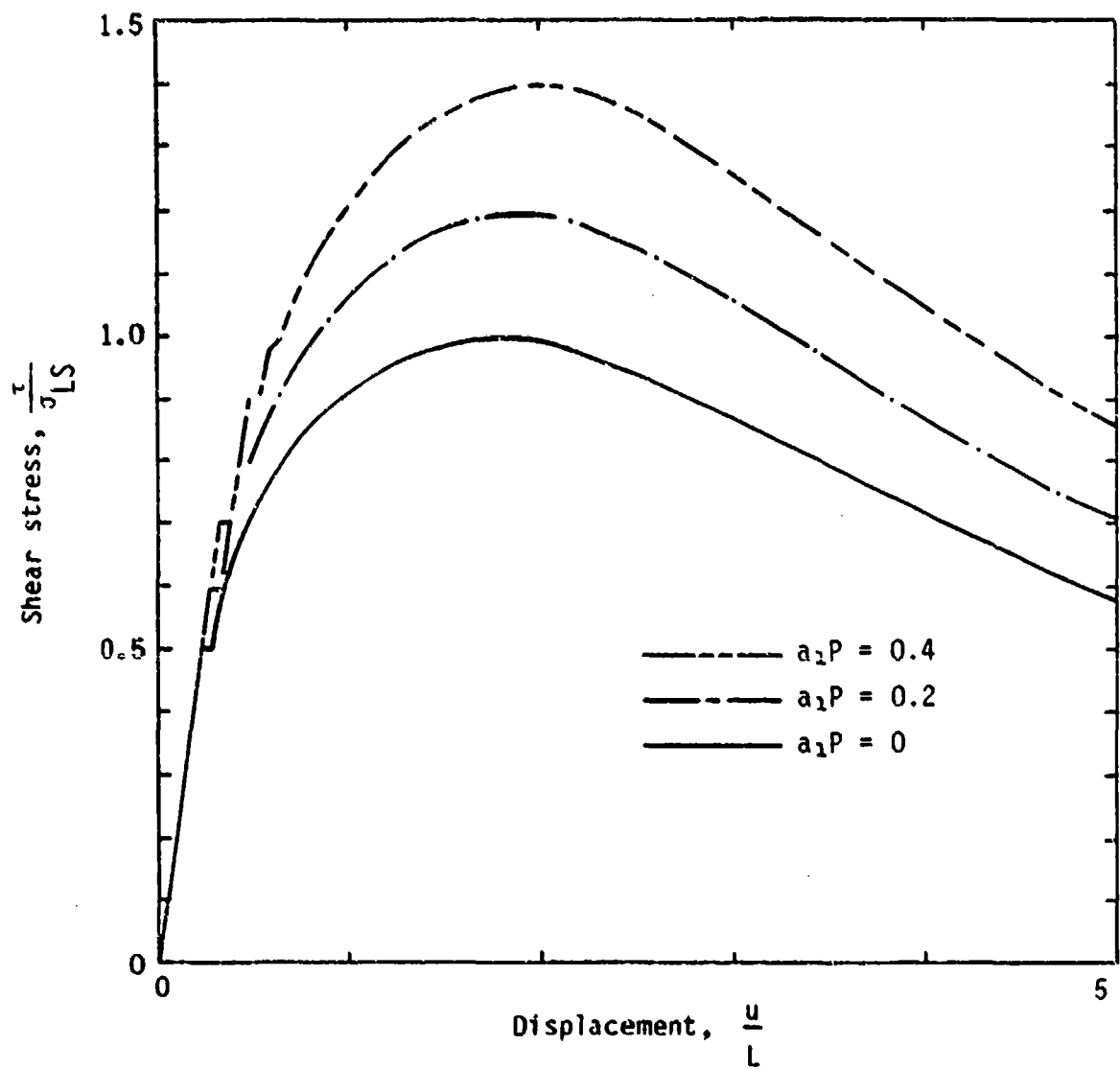


Figure 28. Shear stress versus the displacement of the end of the soil bar for various values of mean pressure.

## V. CONCLUSIONS

It was assumed that no relative slip occurs at the contact surface between soil and concrete. Instead, a shear band appears adjacent to the interface. The shear band is just the physical representation of softening and localization. The interface serves as an initiator of strain softening.

Through numerical testing and indirect comparisons, it was concluded that the new nonlocal constitutive model can simulate the softening behavior of different materials by selecting appropriate values of material parameters. The approach displays the same features as those in Reference 12, but with a much simpler computational procedure. Numerical solutions under dynamic and static shear loadings illustrate the perceived characteristics of a soil-concrete interface.

Because of the difficulties in measuring the localization zone with high strain gradients, existing experimental data are not satisfactory. Once good experimental data are available, it will be necessary to verify the model, not only in one-dimensional, but also in two- and three-dimensional cases such as curved interfaces. Further progress on understanding interface phenomena will require a combination of experimental and theoretical investigations. The research reported here indicates that a nonlocal constitutive model is a promising theoretical approach.

## REFERENCES

1. Huck, P. J., Liber, T., Chiapetta, R. L., Thomopoulos, N. T., and Singh, N. M., **Dynamic Response of Soil/Concrete Interfaces at High Pressure**, Technical Report No. AFWL-TR-73-264, Air Force Weapons Laboratory, Kirtland Air Force Base, NM, 1973.
2. Huck, P. J., and Saxena, S. K., "Response of Soil-Concrete Interface at High Pressure," **Proc. Xth Int. Conf. Soil Mech. Found. Engng.**, Stockholm, Sweden, June, 1981.
3. Drumm, E. C., and Desai, C. S., "Testing and Constitutive Modeling for Interface Behavior in Dynamic Soil-Structure Interaction," Report to National Science Foundation, Washington, D. C., 1983.
4. Vermeer, P. A., "Frictional Slip and Non-associated Plasticity," **Scandinavian Journal of Metallurgy**, Vol. 12, 1983, pp. 268-276.
5. Hadjian, A. H., Luco, J. E., and Tsai, N. C., "Soil-Structure Interaction: Continuum or Finite Elements?", **Nuclear Engineering and Design**, Vol. 31, 1974, pp. 151-167.
6. Seed, H. B., Lysmer, J., and Hwang, R., "Soil-Structure Interaction Analyses for Seismic Response," **Journal of the Geotechnical Engineering Division**, Proceedings of ASCE, Vol. 101, No. G75, May, 1975.
7. Desai, C. S., and Siriwardane, H. J., **Constitutive Laws for Engineering Materials with Emphasis on Geologic Materials**, Prentice-Hall, Inc., 1984.
8. Oden, J. T., and Pires, E. B., "Numerical Analysis of Certain Contact Problems in Elasticity with Non-classical Friction Laws," **Computers and Structures**, Vol. 16, No. 1-4, 1983, pp. 481-485.
9. Valanis, I. C., "On the Uniqueness of Solution of the Initial Value Problem in Strain Softening Materials," **Journal of Applied Mechanics**, Vol. 52, No. 3, September, 1985, pp. 649-653.
10. Sandler, I., and Wright, J., "Summary of Strain-Softening," **Theoretical Foundations for Large-Scale Computations of Nonlinear Material Behavior**, Preprints, DARPA-NSF Workshop, S. Nemat-Nasser, ed., Northwestern University, Evanston, Illinois, October, 1983, pp. 225-241.
11. Read, H. E., and Hegemier, G. A., "Strain Softening of Rock, Soil and Concrete," **Mechanics of Materials** Vol. 3, 1984, pp. 271-294.
12. Bazant, Z. P., Belytschko, T. B., and Chang, T., "Continuum Theory for Strain Softening," **Journal of Engineering Mechanics**, Vol. 110, No. 12, December, 1984.
13. Schreyer, H. L., and Chen, Z., "One-Dimensional Softening with Localization," **Journal of Applied Mechanics**, (accepted for publication).
14. Schreyer, H. L., **The Application of Plasticity and Viscoplasticity to Metals and Frictional Materials**, Course Notes, ME 544, University of New Mexico, 1985.



15. Becker, E. B., Carey, G. F., and Oden, J. T., **Finite Elements--An Introduction**, Prentice-Hall, Inc., 1981.
16. Dhatt, G., and Touzot, G., **The Finite Element Method Displayed**, John Wiley & Sons, Inc., 1984.

# LIST OF SYMBOLS

$e_{ij}$	Total strain tensor
$e_{ij}^{di}$	Inelastic deviatoric strain tensor
$e_{ij}^e$	Elastic strain tensor
$e_{ij}^i$	Inelastic strain tensor
$\bar{e}^i$	Inelastic strain invariant
$\bar{e}_L^i$	Limit value of $\bar{e}^i$
$e_{EL}$	Shear strain at the elastic limit
$E$	Young's modulus
$f_i$	Global force vector
$f_o, f_L$	External loads
$f_i^{le}$	Element internal force vector
$F$	Yield surface function
$G$	Shear modulus
$G_r$	Strain gradient softening function
$H$	Strain hardening and softening function
$\bar{g}^i$	Inelastic strain gradient invariant
$h$	Length of a finite element

$L$	Length of a soil bar
$L_0$	Elastic limit of yield surface
$L_p$	Peak value of yield surface
$M_{ij}^e$	Element mass matrix
$M_{ij}$	Global mass matrix
$n$	Material parameter
$P$	Mean pressure
$s$	Time step in time integration
$u_i$	Global displacement vector
$v_i$	Global velocity vector
$w$	Weighting function
$\gamma$	Engineering shear strain
$\Delta e_{ij}$	Total strain increment tensor
$\Delta e_{ij}^e$	Elastic strain increment tensor
$\Delta e_{ij}^i$	Inelastic strain increment tensor
$\nu$	Poisson's ratio
$\rho$	Mass density
$\sigma_{ij}$	Stress tensor
$\tau$	Engineering shear stress